IJRCS

International Journal of Robotics and Control Systems
Vol. 6, No. 1, 2026, pp. 793-818
ISSN 2775-2658
http://pubs2.ascee.org/index.php/ijrcs

ASCEE

An Efficient Analysis of Fractional Derivatives for Solving the Nonlinear Time-Fractional Kuramoto–Sivashinsky Equation Using the Laplace Transform and Adomian Decomposition Method

Ouidad Boulakour [a,1], Ahcene Merad [a,2], Iqbal Batiha [b,c,3,*], Fares Bekhouche [d,4], Nidal Anakira [e,5], Mohd Taib Shatnawi [f,6], Nourhane Attia [g,7]

[a] Laboratory of Dynamical Systems and Control, Department of Mathematics and Computer Science, University of Oum El Bouaghi, Oum El Bouaghi 04000, Algeria
[b] Department of Mathematics, Al-Zaytoonah University of Jordan, Amman 11733, Jordan
[c] Nonlinear Dynamics Research Center (NDRC), Ajman University, Ajman 346, United Arab Emirates
[d] Laboratory of Mathematics and Artificial Intelligence, Department of Mathematics, Abbes Laghrour University, Khenchela 40000, Algeria
[e] Faculty of Education and Arts, Sohar University, Sohar 3111, Oman
[f] Department of Basic Science, Al-Huson University College, Al-Balqa Applied University, Irbid 21510, Jordan
[g] National High School for Marine Sciences and Coastal(ENSSMAL), Dely Ibrahim University Campus, Bois des Cars, B.P. 19, 16320, Algiers, Algeria
[1] ouidad.boulakour@univ-oeb.dz; [2] ahcene.merad@univ-oeb.dz; [3] i.batiha@zuj.edu.jo;
[4] fares.bekhouche@univ-khenchela.dz; [5] nanakira@su.edu.om; [6] taib.Shatnawi@bau.edu.jo;
[7] nourhane.attia@enssmal.edu.dz
[*] Corresponding Author

ARTICLE INFO

Article History
Received August 26, 2025
Revised October 12, 2025
Accepted March 27, 2026

Keywords
Laplace-Adomian Decomposition Method;
Time-Fractional Derivatives;
Nonlinear Time-Fractional Kuramoto–Sivashinsky Equation;
Convergence Analysis;
Numerical Stability;
Error Estimation

ABSTRACT

This work presents a comparative analysis of the nonlinear time-fractional Kuramoto–Sivashinsky (KS) equation under three fractional derivative operators: Caputo, Caputo–Fabrizio, and Atangana–Baleanu in the Caputo sense. The objective is to examine how these operator definitions affect the qualitative behavior of the KS equation, particularly in terms of stability, damping, and wave propagation. For this purpose, the Laplace–Adomian decomposition method (L-ADM) is employed to construct semi-analytical series solutions expressed as rapidly convergent expansions. A unified framework is developed to apply L-ADM to all three fractional operators, supported by a rigorous convergence, existence, and uniqueness analysis, ensuring the stability and reliability of the obtained solutions. The comparison evaluates absolute error, convergence rate, and computation time to assess both accuracy and efficiency. Two numerical examples are presented for fractional orders α on the solution behavior. The outcomes are further compared with those of the new iterative transform method (NITM) and the q-homotopy analysis transform method (q-HATM). The results demonstrate distinct differences in solution behavior across the three fractional derivatives, emphasizing the importance of operator selection in fractional modeling.

1. Introduction

Fractional calculus has emerged in recent decades as a powerful mathematical framework for modeling systems with memory, nonlocal effects, and hereditary properties [1]–[5]. Unlike classical calculus, which captures only instantaneous dynamics, fractional derivatives incorporate the influence of past states into the formulation [6], [8]–[11]. This makes them particularly suitable for describing phenomena such as anomalous diffusion, viscoelasticity, biological dynamics, fluid mechanics [12]–[16]. As a result, fractional partial differential equations (FPDEs) have gained wide attention in applied mathematics, physics, and engineering, biology, and many other sciences providing more accurate and flexible models for complex processes [17]–[22].

Within this context, the Kuramoto-Sivashinsky (KS) equation stands out as one of the most significant nonlinear models. Originally introduced in the late 1970s to describe flame front instabilities [23], [24], it has since been applied in areas such as thin-film flows, reaction-diffusion systems, turbulence, and crystal growth [25]–[28]. The equation is structurally simple compared to other nonlinear models, yet it exhibits remarkably rich dynamics, including traveling waves, chaos, and spatiotemporal turbulence [29]–[33]. These properties make it an attractive benchmark for testing both analytical and numerical methods [34]–[47].

The time-fractional form of the KS equation can be expressed as:

$$\begin{aligned}\mathcal{D}_{\varrho}^{\alpha}\mathfrak{u}(\zeta,\varrho)+\mathfrak{u}(\zeta,\varrho)\mathcal{D}_{\zeta}\mathfrak{u}(\zeta,\varrho)+\sigma\mathcal{D}_{\zeta\zeta}\mathfrak{u}(\zeta,\varrho)+\eta\mathcal{D}_{\zeta\zeta\zeta}\mathfrak{u}(\zeta,\varrho)\\ +\mu\mathcal{D}_{\zeta\zeta\zeta\zeta}\mathfrak{u}(\zeta,\varrho)=0,\zeta\in\mathbb{R},\varrho\in[0,T],\alpha\in(0,1],\end{aligned} \tag{1}$$

Where σ, η and μ are constants, and $\mathcal{D}^{\alpha}$ represents a fractional derivative operator of order α.

Several fractional derivatives have been proposed in the literature, each with distinct mathematical features and physical interpretations. The Caputo derivative is the most commonly used, as it aligns naturally with traditional initial conditions [48], [49]. The Caputo-Fabrizio derivative eliminates the singular kernel by introducing an exponential kernel, providing smoother solutions and improved numerical stability [50], [51]. The Atangana-Baleanu derivative in the Caputo sense employs a Mittag-Leffler kernel, offering a more general description of memory effects in a nonlocal and nonsingular form [52], [53]. A comparative study of these operators within the same nonlinear model is therefore essential to understand their impact on solution stability, damping, and wave propagation [54]–[56].

The KS equation provides an ideal testbed for fractional derivatives for several reasons. First, its compact structure makes it analytically tractable while still reflecting nonlinear interactions. Second, its ability to generate complex behaviors such as chaos, pattern formation, and spatiotemporal structures offers a natural setting to investigate how different fractional operators influence solution dynamics. Third, because the KS equation is widely applied in fields such as flame propagation, fluid dynamics, and turbulence, extending it into the fractional domain enables deeper insights into the role of memory and nonlocality in real physical systems [57], [59].

Various semi-analytical methods have been proposed to solve FPDEs, including the natural decomposition method (NTDM) [60], and the q-homotopy analysis transform method (q-HATM) [61]. Although effective in certain cases, these methods often suffer from slow convergence or reliance on auxiliary parameters that can be difficult to optimize.

In contrast, the Laplace-Adomian Decomposition Method (L-ADM) combines the strengths of the Laplace transform in handling initial conditions with the flexibility of Adomian polynomials in treating nonlinear terms [62]–[65]. This hybrid structure enables the construction of rapidly convergent series solutions without requiring linearization, discretization, or perturbation.

Moreover, the unified framework of L-ADM allows its systematic application to different fractional operators, making it an optimal choice for conducting a comparative study across multiple definitions of fractional derivatives [66]. However, despite the growing interest in fractional-order mod-

eling, there remains a lack of direct comparative studies on the influence of different fractional derivatives on nonlinear systems, particularly the KS equation, which serves as a benchmark for analyzing instability and pattern formation in complex dynamical processes.

Based on these considerations, the main contributions of this work can be summarized as follows:

- Development of a unified L-ADM framework for solving the fractional KS equation under three different derivative definitions.
- A comparative analysis of the Caputo, Caputo-Fabrizio, and Atangana-Baleanu (Caputo sense) derivatives, highlighting their influence on solution stability and dynamical behavior.
- Existence, uniqueness, and convergence analysis based on the Banach fixed point theorem, ensuring the stability and reliability of the proposed solutions.
- Numerical examples that demonstrate the effectiveness of the method, including a comparative study of the three derivatives in terms of their impact on solution behaviors, alongside benchmarking against NITM and q-HATM to highlight the efficiency and accuracy of L-ADM.

The remainder of this paper is organized as follows. Section 2 presents the essential preliminaries and definitions of the fractional derivatives used in this study. Section 3 describes the unified formulation of the L-ADM. Section 4 provides the existence, uniqueness, and convergence analysis of the L-ADM.

When applied to the fractional KS equation. Section 5 presents two numerical applications of the fractional KS equation and provides comparative analyses of the three fractional derivatives using tables and graphical results. Finally, Section 6 concludes the paper by summarizing the key findings and suggesting directions for future research.

2. Key Principles

This section presents the fundamental concepts of the L-ADM and its application to FPDEs. We begin by introducing the Laplace transform (LT) and its inverse. Subsequently, we examine the definitions and properties of time-fractional derivatives, including the Caputo, Caputo–Fabrizio, and Atangana–Baleanu derivatives in the Caputo sense.

2.1. The Laplace Transform

Definition 1 [66] Assume that $\mathfrak{u}$ is a piecewise continuous (PC) function on $J \times [0;\infty)$ (J is an interval), and of exponential order λ, then the LT of $\mathfrak{u}(\zeta,\varrho)$ is defined as follows:

$$\mathcal{U}(\zeta,\mathfrak{s}) = \mathcal{L}\left[\mathfrak{u}(\zeta,\varrho)\right] = \int_0^{+\infty} e^{-\mathfrak{s}t}\mathfrak{u}(\zeta,\varrho)d\varrho, \quad \mathfrak{s} > \lambda,$$

and the inverse LT of $\mathcal{U}(\zeta,\mathfrak{s})$ is defined as:

$$\mathfrak{u}(\zeta,\varrho) = \mathcal{L}^{-1}\left[\mathcal{U}(\zeta,\mathfrak{s})\right] = \int_{l-i\infty}^{l+i\infty} e^{\mathfrak{s}\varrho}\mathcal{U}(\zeta,\mathfrak{s})d\mathfrak{s}, \quad l = Re(\mathfrak{s}) > l_0,$$

l_0 is sits in the region of the right half-plane where the integral converges.

2.2. The Time-Fractional Caputo Derivative

Definition 2 [66] For a function $\mathfrak{u}$, the time-fractional Caputo derivative of order α ($\alpha > 0$) is defined as follows:

$${}^{C}\mathcal{D}_{\varrho}^{\alpha}\mathfrak{u}(\zeta,\varrho) = \frac{d^{\alpha}\mathfrak{u}(\zeta,\varrho)}{d\varrho^{\alpha}} = \begin{cases} \mathcal{I}_{\varrho}^{n-\alpha}(d_{\varrho}^{n}\mathfrak{u}(\zeta,\varrho)), & n-1 < \alpha < n, \\ d_{\varrho}^{n}\mathfrak{u}(\zeta,\varrho), & \alpha = n \in \mathbb{N}. \end{cases}$$

Where $n = [\alpha]+1$ ($[\alpha]$ is the integer part of α), $\varrho \geq 0$, $\zeta \in J$, $d_{\varrho}^{n} = \dfrac{d^n}{d\varrho^n}$, and $\mathcal{I}_{\varrho}^{\beta}$ is the time-fractional Riemann-Liouville integral of order β that given by:

$$\mathcal{I}_{\varrho}^{\beta}\mathfrak{u}(\zeta,\varrho) = \begin{cases} \frac{1}{\Gamma(\beta)}\int_0^{\varrho}(\varrho-\tau)^{\beta-1}\mathfrak{u}(\zeta,\tau)d\tau, & \beta > 0,\ 0 \leq \tau < \varrho, \\ \mathfrak{u}(\zeta,\varrho), & \beta = 0. \end{cases}$$

Propertie 1 [66] Assuming that $\mathfrak{u}$ is a PC function of exponential order λ, the LT of the time-fractional Caputo derivative is given by the following formula:

$$\mathcal{L}\left[{}^{C}\mathcal{D}_{\varrho}^{\alpha}\mathfrak{u}(\zeta,\varrho)\right] = \mathfrak{s}^{\alpha}\mathcal{U}(\zeta,\mathfrak{s}) - \mathfrak{s}^{\alpha-1}\mathfrak{u}(\zeta,0),\ \ 0 < \alpha \leq 1. \tag{2}$$

2.3. The Time-Fractional Caputo–Fabrizio Derivative

Definition 3 [66] For a function $\mathfrak{u}$, the time-fractional Caputo–Fabrizio derivative of order α is defined as follows:

$${}^{CF}\mathcal{D}_{\varrho}^{\alpha}\mathfrak{u}(\zeta,\varrho) = \frac{\mathscr{S}(\alpha)}{1-\alpha}\int_0^{\varrho}\frac{du(\zeta,\tau)}{d\tau}e^{-\frac{\alpha}{1-\alpha}(\varrho-\tau)}d\tau,\ \ \varrho > 0,\ 0 < \alpha \leq 1,$$

Where $\mathscr{S}$ represents a normalization function that satisfies $\mathscr{S}(\alpha) = (1-\alpha) + \dfrac{\alpha}{\Gamma(\alpha)}$ with $\mathscr{S}(0) = \mathscr{S}(1) = 1$.

Propertie 2 [66] Assuming that $\mathfrak{u}$ is a PC function of exponential order λ, the LT of the time-fractional Caputo–Fabrizio derivative is given by the following formula:

$$\mathcal{L}\left[{}^{CF}\mathcal{D}_{\varrho}^{\alpha}\mathfrak{u}(\zeta,\varrho)\right] = \mathscr{S}(\alpha)\frac{\mathfrak{s}\,\mathcal{U}(\zeta,\mathfrak{s}) - \mathfrak{u}(\zeta,0)}{\mathfrak{s}+(1-\mathfrak{s})\alpha},\ \ 0 < \alpha \leq 1. \tag{3}$$

2.4. The Time-Fractional Atangana–Baleanu Derivative in the Caputo Sense

Definition 4 The following series represents the Mittag–Leffler function:

$$E_{\alpha}(z) = \sum_{j=0}^{\infty}\frac{z^j}{\Gamma(\alpha j+1)},$$

Where $\alpha > 0$, $z \in \mathbb{C}$, and $\Gamma(.)$ is the Gamma function.

Definition 5 [66] For a function $\mathfrak{u}$, the time-fractional Atangana–Baleanu derivative in the Caputo sense of order α is defined as follows:

$${}^{ABC}\mathcal{D}_{\varrho}^{\alpha}\mathfrak{u}(\zeta,\varrho) = \frac{\mathscr{S}(\alpha)}{1-\alpha}\int_0^{\varrho}\frac{du(\zeta,\tau)}{d\tau}E_{\alpha}(-\frac{\alpha}{1-\alpha}(\varrho-\tau)^{\alpha})d\tau,\ \ \varrho > 0,\ 0 < \alpha \leq 1.$$

Propertie 3 [66] Assuming that $\mathfrak{u}$ is a PC function of exponential order λ, the LT of the time-fractional Atangana–Baleanu derivative in the Caputo sense is given by the following formula:

$$\mathcal{L}\left[{}^{ABC}\mathcal{D}_{\varrho}^{\alpha}\mathfrak{u}(\zeta,\varrho)\right] = \mathscr{S}(\alpha)\frac{\mathfrak{s}^{\alpha}\,\mathcal{U}(\zeta,\mathfrak{s}) - \mathfrak{s}^{\alpha-1}\mathfrak{u}(\zeta,0)}{\alpha+(1-\alpha)\mathfrak{s}^{\alpha}},\ \ 0 < \alpha \leq 1. \tag{4}$$

3. Laplace–Adomian Decomposition Method: Procedural Framework

This section delineates the algorithmic framework of L-ADM, illustrating its application to the general form of nonlinear time-FPDEs and utilizing several types of fractional derivatives, including Caputo, Caputo–Fabrizio, and Atangana–Baleanu in the Caputo sense.

We consider the general nonlinear time-FPDE of the form:

$$\mathcal{D}_{\varrho}^{\alpha}\mathfrak{u}(\zeta,\varrho)+\mathscr{L}\left[\mathfrak{u}(\zeta,\varrho)\right]+\mathscr{N}\left[\mathfrak{u}(\zeta,\varrho)\right]=f(\zeta,\varrho), \tag{5}$$

under the initial condition:

$$\mathfrak{u}(\zeta,0)=\mathfrak{u}_0(\zeta), \tag{6}$$

Where $\mathcal{D}_{\varrho}^{\alpha}$ denotes the time-fractional derivative (in the sense of Caputo, Caputo-Fabrizio, or Atangana–Baleanu-Caputo), $\mathscr{L}$ is a linear operator, $\mathscr{N}$ a nonlinear operator, and f a given source function.

To solve the initial value problem (IVP) (5)-(6) using the L-ADM, the following steps are performed:

Step 1. Applying the LT to both sides of equation (5) gives:

$$\mathcal{L}\left[\mathcal{D}_{\varrho}^{\alpha}\mathfrak{u}(\zeta,\varrho)\right]=\mathcal{L}[f(\zeta,\varrho)-\mathscr{L}[\mathfrak{u}(\zeta,\varrho)]-\mathscr{N}[\mathfrak{u}(\zeta,\varrho)]]\,.$$

Depending on the type of fractional derivative, the LT of $\mathcal{D}_{\varrho}^{\alpha}\mathfrak{u}$ takes a different form, summarized in the following table, where $\mathcal{U}(\zeta,\mathfrak{s})=\mathcal{L}\left[\mathfrak{u}(\zeta,\varrho)\right]$ shown in Table 1:

Table 1. Laplace transforms of different fractional derivatives

Fractional Derivative	LT expression ($\mathcal{L}\left[\mathcal{D}_{\varrho}^{\alpha}\mathfrak{u}(\zeta,\varrho)\right]$)
Caputo	$\mathfrak{s}^{\alpha}\mathcal{U}(\zeta,\mathfrak{s})-\mathfrak{s}^{\alpha-1}\mathfrak{u}(\zeta,0)$
Caputo-Fabrizio	$\frac{\mathscr{S}(\alpha)(\mathfrak{s}\,\mathcal{U}(\zeta,\mathfrak{s})-\mathfrak{u}(\zeta,0))}{\mathfrak{s}+\alpha(1-\mathfrak{s})}$
Atangana-Baleanu (Caputo sense)	$\frac{\mathscr{S}(\alpha)(\mathfrak{s}^{\alpha}\mathcal{U}(\zeta,\mathfrak{s})-\mathfrak{s}^{\alpha-1}\mathfrak{u}(\zeta,0))}{\mathfrak{s}^{\alpha}+\alpha(1-\mathfrak{s}^{\alpha})}$

Step 2. After isolating $\mathcal{U}(\zeta,\mathfrak{s})$, we obtain the following equation:

$$\mathcal{U}(\zeta,\mathfrak{s})=\frac{\mathfrak{u}_0(\zeta)}{\mathfrak{s}}+\mathcal{F}(\mathfrak{s})\cdot\mathcal{L}[f(\zeta,\varrho)-\mathscr{L}[\mathfrak{u}(\zeta,\varrho)]-\mathscr{N}[\mathfrak{u}(\zeta,\varrho)]]\,, \tag{7}$$

Where $\mathcal{F}(\mathfrak{s})$ is an auxiliary expression depending on the type of derivative. Its form is summarized as follows shown in Table 2:

Table 2. Auxiliary functions $\mathcal{F}(\mathfrak{s})$ for different fractional derivative definitions

Fractional Derivative	Auxiliary Function $\mathcal{F}(\mathfrak{s})$
Caputo	$\frac{1}{\mathfrak{s}^{\alpha}}$
Caputo-Fabrizio	$\frac{\alpha+\mathfrak{s}(1-\alpha)}{\mathfrak{s}.\mathscr{S}(\alpha)}$
Atangana-Baleanu (Caputo sense)	$\frac{\alpha+\mathfrak{s}^{\alpha}(1-\alpha)}{\mathfrak{s}^{\alpha}\mathscr{S}(\alpha)}$

Step 3. Taking the inverse LT of equation (7), we obtain:

$$\mathfrak{u}(\zeta,\varrho)=\mathfrak{u}_0(\zeta)+\mathcal{L}^{-1}[\mathcal{F}(\mathfrak{s})\cdot\mathcal{L}[f(\zeta,\varrho)]]-\mathcal{L}^{-1}[\mathcal{F}(\mathfrak{s})\cdot\mathcal{L}[\mathscr{L}[\mathfrak{u}(\zeta,\varrho)]+\mathscr{N}[\mathfrak{u}(\zeta,\varrho)]]]\,. \tag{8}$$

Step 4. The solution is expressed as an infinite series:

$$\mathfrak{u}(\zeta,\varrho)=\sum_{n=0}^{\infty}\mathfrak{u}_n(\zeta,\varrho), \tag{9}$$

while the nonlinear operator is decomposed into Adomian polynomials:

$$\mathscr{N}[\mathfrak{u}(\zeta,\varrho)] = \sum_{n=0}^{\infty} \mathscr{A}_n(\zeta,\varrho), \tag{10}$$

with,

$$\mathscr{A}_n(\zeta,\varrho) = \mathscr{A}_n(\mathfrak{u}_0(\zeta,\varrho),\mathfrak{u}_1(\zeta,\varrho),\ldots,\mathfrak{u}_n(\zeta,\varrho)) = \frac{1}{n!}\frac{d^n}{d\chi^n}\mathscr{N}\left(\sum_{k=0}^{n}\chi^k\mathfrak{u}_k(\zeta,\varrho)\right)\Bigg|_{\chi=0}.$$

Step 5. Inserting equations (10) and (9) into equation (8) gives:

$$\sum_{n=0}^{\infty}\mathfrak{u}_n(\zeta,\varrho) = \mathcal{G}(\zeta,\varrho) - \mathcal{L}^{-1}\left[\mathcal{F}(\mathfrak{s})\cdot\mathcal{L}\left[\mathscr{L}\left[\sum_{n=0}^{\infty}\mathfrak{u}_n(\zeta,\varrho)\right] + \sum_{n=0}^{\infty}\mathscr{A}_n(\zeta,\varrho)\right]\right], \tag{11}$$

Where:

$$\mathcal{G}(\zeta,\varrho) = \mathfrak{u}_0(\zeta) + \mathcal{L}^{-1}[\mathcal{F}(\mathfrak{s})\cdot\mathcal{L}[f(\zeta,\varrho)]]\,.$$

Step 6. The following result can be obtained by comparing the two sides of equation (11):

$$\begin{cases}\mathfrak{u}_0(\zeta,\varrho) = \mathcal{G}(\zeta,\varrho),\\ \mathfrak{u}_{n+1}(\zeta,\varrho) = -\mathcal{L}^{-1}\left[\mathcal{F}(\mathfrak{s})\cdot\mathcal{L}\left[\mathscr{L}\left[\mathfrak{u}_n(\zeta,\varrho)\right] + \mathscr{A}_n(\zeta,\varrho)\right]\right], \quad n\geq 0.\end{cases} \tag{12}$$

Step 7. Finally, we find the L-ADM solution to the+ IVP (5)-(6) by calculating the terms $\mathfrak{u}_0(\zeta,\varrho)$, $\mathfrak{u}_1(\zeta,\varrho)$, $\mathfrak{u}_2(\zeta,\varrho)$, ... of the recurrence sequence (12) and using relation (9).

Remark 1 The L-ADM provides semi-analytical solutions, since each term $\mathfrak{u}_n(\zeta,\varrho)$ is derived analytically in a series form, while the complete solution is obtained by truncating the infinite series after a finite number of terms, which introduces a numerical aspect. In this way, the method effectively combines analytical formulation with numerical approximation.

For a clearer understanding of the proposed procedure, the above steps are summarized in the following flowchart shown in Fig. 1:

4. Existence, Uniqueness, and Convergence Analysis

This section establishes the mathematical validity of the proposed approach by proving the existence, uniqueness, and convergence of the solution to the fractional KS equation. Using the Banach fixed point theorem, it is shown that the L-ADM yields a unique and uniformly convergent solution within a suitable Banach space.

Theorem 1 [existence and uniqueness] Let $\mathcal{X} = C(\mathbb{R}\times[0,T])$ be the Banach space of continuous functions on $\mathbb{R}\times[0,T]$, equipped with the sup norm:

$$\|\mathfrak{u}\| = \sup_{(\zeta,\varrho)\in\mathbb{R}\times[0,T]} |\mathfrak{u}(\zeta,\varrho)|.$$

Define the operator $\mathcal{H}:\mathcal{X}\to\mathcal{X}$, through which the fractional KS equation can be written in fixed point form:

$$\mathfrak{u}(\zeta,\varrho) = \mathcal{H}\mathfrak{u}(\zeta,\varrho),$$

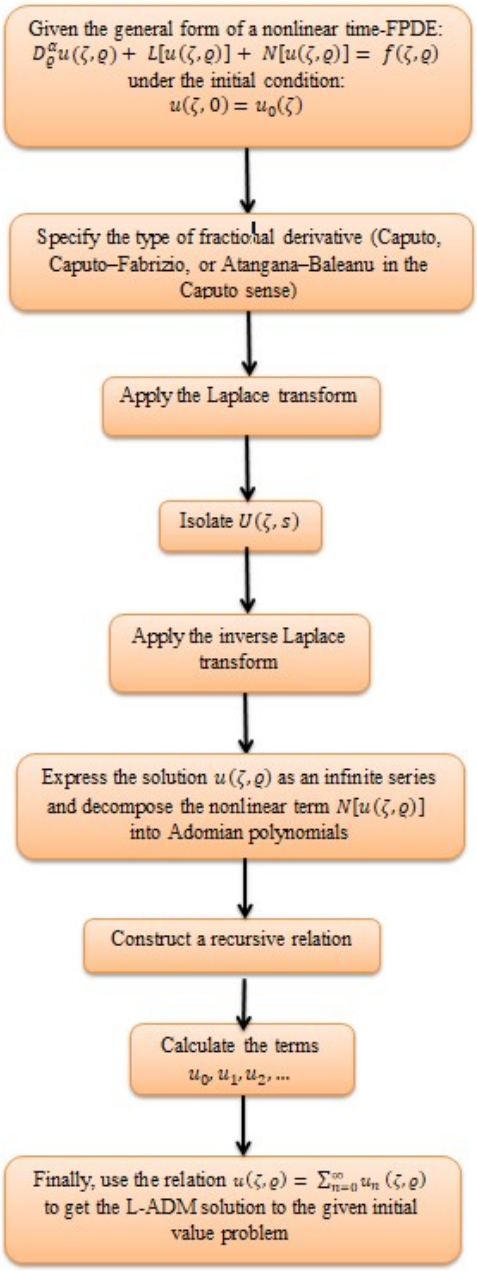

Fig. 1. Stepwise flowchart of the Laplace–Adomian decomposition method

Where,

$$\mathcal{H}\mathfrak{u} = \mathfrak{u}_0 - \mathcal{L}^{-1}\left[\mathcal{F}(\mathfrak{s}) \cdot \mathcal{L}\left[\sigma\mathcal{D}_{\zeta\zeta}\mathfrak{u} + \eta\mathcal{D}_{\zeta\zeta\zeta}\mathfrak{u} + \mu\mathcal{D}_{\zeta\zeta\zeta\zeta}\mathfrak{u} + \mathfrak{u}\mathcal{D}_{\zeta}\mathfrak{u}\right]\right].$$

Here, $\mathcal{F}(\mathfrak{s})$ denotes the auxiliary function associated with the chosen fractional derivative (see Table 2).

Assume that:

1. The linear spatial operators and nonlinear term are Lipschitz continuous. That is, there exist constants $L_2, L_3, L_4, L_N > 0$ such that, for all $\mathfrak{u}, \mathfrak{v} \in \mathcal{X}$:

$$\|\mathcal{D}_\zeta^k\mathfrak{u} - \mathcal{D}_\zeta^k\mathfrak{v}\| \leq L_k\|\mathfrak{u} - \mathfrak{v}\|, \quad k = 2, 3, 4,$$

$$\| \mathfrak{u}\,\mathcal{D}_\zeta \mathfrak{u} - \mathfrak{v}\,\mathcal{D}_\zeta \mathfrak{v} \| \leq L_N \|\mathfrak{u} - \mathfrak{v}\|.$$

2. Define;

$$L = sup\Big(L_2|\sigma|, L_3|\eta|,\ L_4|\mu|,\ L_N\Big), \quad \kappa = L \cdot \mathcal{L}^{-1}\left[\frac{\mathcal{F}(\mathfrak{s})}{\mathfrak{s}}\right].$$

If $0 \leq \kappa < 1$, then the operator $\mathcal{H}$ is a contraction on $\mathcal{X}$.

Under these assumptions, the operator $\mathcal{H}$ admits a unique fixed point $\mathfrak{u}^* \in \mathcal{X}$; this fixed point is the unique continuous solution of the fractional KS equation on $\mathbb{R} \times [0, T]$.

Proof. Let $\mathfrak{u}$ and $\mathfrak{v}$ be two functions in $\mathcal{X}$. From the definition of the operator $\mathcal{H}$, we have:

$$\begin{aligned}
|\mathcal{H}\mathfrak{u} - \mathcal{H}\mathfrak{v}| &= \left| \begin{array}{l} \mathcal{L}^{-1}\Big[\mathcal{F}(\mathfrak{s}) \cdot \mathcal{L}\Big[\sigma \mathcal{D}_{\zeta\zeta}\mathfrak{u} + \eta \mathcal{D}_{\zeta\zeta\zeta\zeta}\mathfrak{u} + \mu \mathcal{D}_{\zeta\zeta\zeta\zeta\zeta}\mathfrak{u} + \mathfrak{u}\mathcal{D}_\zeta \mathfrak{u}\Big]\Big] \\ \quad - \mathcal{L}^{-1}\Big[\mathcal{F}(\mathfrak{s}) \cdot \mathcal{L}\Big[\sigma \mathcal{D}_{\zeta\zeta}\mathfrak{v} + \eta \mathcal{D}_{\zeta\zeta\zeta\zeta}\mathfrak{v} + \mu \mathcal{D}_{\zeta\zeta\zeta\zeta\zeta}\mathfrak{v} + \mathfrak{v}\mathcal{D}_\zeta \mathfrak{v}\Big]\Big] \end{array} \right| \\
&= \left| \begin{array}{l} \sigma \mathcal{L}^{-1}\Big[\mathcal{F}(\mathfrak{s}) \cdot \mathcal{L}\Big[\mathcal{D}_{\zeta\zeta}\mathfrak{u} - \mathcal{D}_{\zeta\zeta}\mathfrak{v}\Big]\Big] + \eta \mathcal{L}^{-1}\Big[\mathcal{F}(\mathfrak{s}) \cdot \mathcal{L}\Big[\mathcal{D}_{\zeta\zeta\zeta\zeta}\mathfrak{u} - \mathcal{D}_{\zeta\zeta\zeta\zeta}\mathfrak{v}\Big]\Big] \\ + \mu \mathcal{L}^{-1}\Big[\mathcal{F}(\mathfrak{s}) \cdot \mathcal{L}\Big[\mathcal{D}_{\zeta\zeta\zeta\zeta\zeta}\mathfrak{u} - \mathcal{D}_{\zeta\zeta\zeta\zeta\zeta}\mathfrak{v}\Big]\Big] + \mathcal{L}^{-1}\Big[\mathcal{F}(\mathfrak{s}) \cdot \mathcal{L}\Big[\mathfrak{u}\mathcal{D}_\zeta \mathfrak{u} - \mathfrak{v}\mathcal{D}_\zeta \mathfrak{v}\Big]\Big] \end{array} \right| \\
&\leq \left[\begin{array}{l} |\sigma|\, \mathcal{L}^{-1}\Big[\mathcal{F}(\mathfrak{s}) \cdot \mathcal{L}\Big[\,|\mathcal{D}_{\zeta\zeta}\mathfrak{u} - \mathcal{D}_{\zeta\zeta}\mathfrak{v}|\,\Big]\Big] + |\eta|\, \mathcal{L}^{-1}\Big[\mathcal{F}(\mathfrak{s}) \cdot \mathcal{L}\Big[\,|\mathcal{D}_{\zeta\zeta\zeta\zeta}\mathfrak{u} - \mathcal{D}_{\zeta\zeta\zeta\zeta}\mathfrak{v}|\,\Big]\Big] \\ + |\mu|\, \mathcal{L}^{-1}\Big[\mathcal{F}(\mathfrak{s}) \cdot \mathcal{L}\Big[\,|\mathcal{D}_{\zeta\zeta\zeta\zeta\zeta}\mathfrak{u} - \mathcal{D}_{\zeta\zeta\zeta\zeta\zeta}\mathfrak{v}|\,\Big]\Big] + \mathcal{L}^{-1}\Big[\mathcal{F}(\mathfrak{s}) \cdot \mathcal{L}\Big[\,|\mathfrak{u}\mathcal{D}_\zeta \mathfrak{u} - \mathfrak{v}\mathcal{D}_\zeta \mathfrak{v}|\,\Big]\Big] \end{array} \right]
\end{aligned}$$

Taking sup norms and using the Lipschitz bounds yields:

$$\begin{aligned}
\|\mathcal{H}\mathfrak{u} - \mathcal{H}\mathfrak{v}\| &\leq \left[\begin{array}{l} L_2\,|\sigma|\, \mathcal{L}^{-1}\Big[\mathcal{F}(\mathfrak{s}) \cdot \mathcal{L}\Big[\,\|\mathfrak{u} - \mathfrak{v}\|\,\Big]\Big] + L_3\,|\eta|\, \mathcal{L}^{-1}\Big[\mathcal{F}(\mathfrak{s}) \cdot \mathcal{L}\Big[\,\|\mathfrak{u} - \mathfrak{v}\|\,\Big]\Big] \\ + L_4\,|\mu|\, \mathcal{L}^{-1}\Big[\mathcal{F}(\mathfrak{s}) \cdot \mathcal{L}\Big[\,\|\mathfrak{u} - \mathfrak{v}\|\,\Big]\Big] + L_N \mathcal{L}^{-1}\Big[\mathcal{F}(\mathfrak{s}) \cdot \mathcal{L}\Big[\,\|\mathfrak{u} - \mathfrak{v}\|\,\Big]\Big] \end{array} \right] \\
&\leq L \cdot \mathcal{L}^{-1}\Big[\mathcal{F}(s) \cdot \mathcal{L}\Big[\,\|\mathfrak{u} - \mathfrak{v}\|\,\Big]\Big] \\
&\leq L \cdot\ \mathcal{L}^{-1}\left[\frac{\mathcal{F}(s)}{s}\right] \|\mathfrak{u} - \mathfrak{v}\| \\
&\leq \kappa\, \|\mathfrak{u} - \mathfrak{v}\|
\end{aligned}$$

Since $0 \leq \kappa < 1$ by assumption, the operator $\mathcal{H}$ satisfies the contraction property on $\mathcal{X}$. Therefore, by the Banach fixed point theorem, $\mathcal{H}$ possesses a unique fixed point $\mathfrak{u}^* \in \mathcal{X}$. This fixed point corresponds to the unique continuous solution of the fractional KS equation on $\mathbb{R} \times [0, T]$. Furthermore, the value of the contraction constant κ depends explicitly on the type of fractional derivative employed through the auxiliary function $\mathcal{F}(\mathfrak{s})$. The following Table summarizes the corresponding expressions of κ shown in Table 3:

Table 3. Values of the contraction constant κ for different fractional derivatives

Fractional derivative	**Expression of κ**
Caputo	$\dfrac{L\,t^\alpha}{\Gamma(\alpha+1)}$
Caputo–Fabrizio	$\dfrac{L.\Big(1+\alpha+\alpha t\Big)}{\mathscr{S}(\alpha)}$
Atangana-Baleanu (Caputo sense)	$\dfrac{L.\Big((1+\alpha)\Gamma(1+\alpha)+\alpha t^\alpha\Big)}{\Gamma(1+\alpha).\mathscr{S}(\alpha)}$

Theorem 2 [convergence] Let the assumptions of the existence and uniqueness theorem hold. Assume that the operator $\mathcal{H} : \mathcal{X} \to \mathcal{X}$ is a contraction mapping with a contraction constant κ. Then, the sequence of partial sums:

$$\mathbb{S}_n(\zeta, \varrho) = \sum_{k=0}^{n} \mathfrak{u}_k(\zeta, \varrho),$$

Constructed by the L-ADM, forms a Cauchy sequence in the Banach space $\mathcal{X}$. Consequently, the L-ADM series converges uniformly to the unique fixed point $\mathfrak{u}^* \in \mathcal{X}$, which represents the exact continuous solution of the fractional KS equation on $\mathbb{R} \times [0, T]$.

Proof. We first demonstrate that the sequence $\{\mathbb{S}_n\}$ forms a Cauchy sequence in the Banach space $\mathcal{X}$. The nonlinear operator $\mathfrak{u}\,\mathcal{D}_\zeta \mathfrak{u}$ can be decomposed into a series of Adomian polynomials as:

$$\mathfrak{u}(\zeta, \varrho)\,\mathcal{D}_\zeta \mathfrak{u}(\zeta, \varrho) = \sum_{n=0}^{\infty} \mathscr{A}_n(\zeta, \varrho).$$

Now, we compute:

$$\begin{aligned}
|\mathbb{S}_n - \mathbb{S}_q| &= \left| \sum_{k=q+1}^{n} \mathfrak{u}_k \right| \\
&= \left| \mathcal{L}^{-1}\left[\mathcal{F}(\mathfrak{s}) \cdot \mathcal{L}\Big[\sigma \sum_{k=q+1}^{n} \mathcal{D}_{\zeta\zeta}\mathfrak{u}_{k-1} + \eta \sum_{k=q+1}^{n} \mathcal{D}_{\zeta\zeta\zeta}\mathfrak{u}_{k-1} + \mu \sum_{k=q+1}^{n} \mathcal{D}_{\zeta\zeta\zeta\zeta}\mathfrak{u}_{k-1} + \sum_{k=q+1}^{n} \mathscr{A}_{k-1} \Big] \right] \right| \\
&= \left| \mathcal{L}^{-1}\left[\mathcal{F}(\mathfrak{s}) \cdot \mathcal{L}\Big[\sigma \mathcal{D}_{\zeta\zeta} \left(\sum_{k=q}^{n-1} \mathfrak{u}_k \right) + \eta \mathcal{D}_{\zeta\zeta\zeta} \left(\sum_{k=q}^{n-1} \mathfrak{u}_k \right) + \mu \mathcal{D}_{\zeta\zeta\zeta\zeta} \left(\sum_{k=q}^{n-1} \mathfrak{u}_k \right) + \sum_{k=q}^{n-1} \mathscr{A}_k \Big] \right] \right| \\
&= \left| \begin{array}{l} \mathcal{L}^{-1}\Big[\mathcal{F}(\mathfrak{s}) \cdot \mathcal{L}\Big[\sigma \mathcal{D}_{\zeta\zeta} \left(\mathbb{S}_{n-1} - \mathbb{S}_{q-1} \right) + \eta \mathcal{D}_{\zeta\zeta\zeta} \left(\mathbb{S}_{n-1} - \mathbb{S}_{q-1} \right) + \mu \mathcal{D}_{\zeta\zeta\zeta\zeta} \left(\mathbb{S}_{n-1} - \mathbb{S}_{q-1} \right) \\ + \left(\mathscr{N}\left(\mathcal{S}_{n-1} \right) - \mathscr{N}\left(\mathcal{S}_{q-1} \right) \right) \Big] \Big] \end{array} \right| \\
&\leq \left[\begin{array}{l} |\sigma|\, \mathcal{L}^{-1}\Big[\mathcal{F}(\mathfrak{s}) \cdot \mathcal{L}\Big[\left| \mathcal{D}_{\zeta\zeta}\mathbb{S}_{n-1} - \mathcal{D}_{\zeta\zeta}\mathbb{S}_{q-1} \right| \Big] \Big] + |\eta|\, \mathcal{L}^{-1}\Big[\mathcal{F}(\mathfrak{s}) \cdot \mathcal{L}\Big[\left| \mathcal{D}_{\zeta\zeta\zeta}\mathbb{S}_{n-1} - \mathcal{D}_{\zeta\zeta\zeta}\mathbb{S}_{q-1} \right| \Big] \Big] \\ + |\mu|\, \mathcal{L}^{-1}\Big[\mathcal{F}(\mathfrak{s}) \cdot \mathcal{L}\Big[\left| \mathcal{D}_{\zeta\zeta\zeta\zeta}\mathbb{S}_{n-1} - \mathcal{D}_{\zeta\zeta\zeta\zeta}\mathbb{S}_{q-1} \right| \Big] \Big] + \mathcal{L}^{-1}\Big[\mathcal{F}(s) \cdot \mathcal{L}\Big[\left| \mathbb{S}_{n-1}\mathcal{D}_\zeta \mathbb{S}_{n-1} \right. \\ \left. - \mathbb{S}_{q-1}\mathcal{D}_\zeta \mathbb{S}_{q-1} \right| \Big] \Big] \end{array} \right]
\end{aligned}$$

Applying the sup norms and Lipschitz conditions, we get:

$$\begin{aligned}
\|\mathbb{S}_n - \mathbb{S}_q\| &\leq \left[\begin{array}{l} L_2\, |\sigma|\, \mathcal{L}^{-1}\Big[\mathcal{F}(\mathfrak{s}) \cdot \mathcal{L}\Big[\|\mathbb{S}_{n-1} - \mathbb{S}_{q-1}\| \Big] \Big] + L_3\, |\eta|\, \mathcal{L}^{-1}\Big[\mathcal{F}(\mathfrak{s}) \cdot \mathcal{L}\Big[\|\mathbb{S}_{n-1} - \mathbb{S}_{q-1}\| \Big] \Big] \\ + L_4\, |\mu|\, \mathcal{L}^{-1}\Big[\mathcal{F}(\mathfrak{s}) \cdot \mathcal{L}\Big[\|\mathbb{S}_{n-1} - \mathbb{S}_{q-1}\| \Big] \Big] + L_N \mathcal{L}^{-1}\Big[\mathcal{F}(\mathfrak{s}) \cdot \mathcal{L}\Big[|\mathbb{S}_{n-1} - \mathbb{S}_{q-1}| \Big] \Big] \end{array} \right] \\
&\leq L \cdot \mathcal{L}^{-1}\Big[\mathcal{F}(\mathfrak{s}) \cdot \mathcal{L}\Big[\|\mathbb{S}_{n-1} - \mathbb{S}_{q-1}\| \Big] \Big] \\
&\leq L \cdot\ \mathcal{L}^{-1}\left[\frac{\mathcal{F}(\mathfrak{s})}{\mathfrak{s}} \right] \|\mathbb{S}_{n-1} - \mathbb{S}_{q-1}\| \\
&\leq \kappa \left\| \mathbb{S}_{n-1} - \mathbb{S}_{q-1} \right\|.
\end{aligned}$$

Substituting $n = q + 1$ into the contraction inequality yields the following successive-difference estimate:

$$\begin{aligned}\|\mathbb{S}_{q+1} - \mathbb{S}_q\| &\leq \kappa \|\mathbb{S}_q - \mathbb{S}_{q-1}\| \\ &\leq \kappa^2 \|\mathbb{S}_{q-1} - \mathbb{S}_{q-2}\| \\ &\leq \kappa^3 \|\mathbb{S}_{q-2} - \mathbb{S}_{q-3}\| \\ &\vdots \\ &\leq \kappa^q \|\mathbb{S}_1 - \mathbb{S}_0\|.\end{aligned}$$

For arbitrary $n > q$, we write:

$$\mathbb{S}_n - \mathbb{S}_q = \sum_{k=q}^{n-1} (\mathbb{S}_{k+1} - \mathbb{S}_k).$$

Taking the sup norms and using the geometric bound yields:

$$\|\mathbb{S}_n - \mathbb{S}_q\| \leq \sum_{k=q}^{n-1} \|\mathbb{S}_{k+1} - \mathbb{S}_k\| \leq \sum_{k=q}^{n-1} \kappa^k \|\mathbb{S}_1 - \mathbb{S}_0\|.$$

Letting $n \to \infty$ and summing the geometric series gives:

$$\|\mathbb{S}_n - \mathbb{S}_q\| \leq \sum_{k=q}^{\infty} \kappa^k \|\mathbb{S}_1 - \mathbb{S}_0\| = \frac{\kappa^q}{1-\kappa} \|\mathbb{S}_1 - \mathbb{S}_0\|.$$

Because $0 \leq \kappa < 1$, the right-hand side of the inequality tends to zero as $q \to \infty$. Consequently, the sequence $\{\mathbb{S}_n\}$ is Cauchy in the complete Banach space $\mathcal{X}$ and therefore converges uniformly to a limit $\mathfrak{u}^* \in \mathcal{X}$. Moreover, by the continuity of the operator $\mathcal{H}$ and the recursive construction of the sequence, it follows that $\mathcal{H}(\mathfrak{u}^*) = \mathfrak{u}^*$. Hence, $\mathfrak{u}^*$ represents the unique fixed point of $\mathcal{H}$, and thus corresponds to the unique continuous solution of the fractional KS equation on $\mathbb{R} \times [0, T]$. As an immediate corollary, the truncation (error) bound for the N-th partial sum follows:

$$\|\mathfrak{u}^* - \mathbb{S}_N\| \leq \frac{\kappa^N}{1-\kappa} \|\mathbb{S}_1 - \mathbb{S}_0\|.$$

Remark 2 The established uniqueness and convergence results imply the stability of the L-ADM when applied to the fractional KS equation.

5. Numerical Implementation

This section investigates the numerical implementation of the L-ADM for solving the fractional KS problem with different values of σ, η, and μ. Through these implementations, we examine the efficiency, accuracy, and convergence of L-ADM, as well as the influence of different fractional derivatives — including Caputo, Caputo–Fabrizio, and Atangana–Baleanu (in the Caputo sense) — on the behavior of the solution.

5.1. Application 1

We apply the L-ADM to fractional KS equation with the fixed parameters $\sigma = 1$, $\eta = 0$ and $\mu = 1$. With these values, the governing model is written in the form:

$$\mathcal{D}_\varrho^\alpha \mathfrak{u}(\zeta, \varrho) + \mathfrak{u}(\zeta, \varrho)\mathcal{D}_\zeta \mathfrak{u}(\zeta, \varrho) + \mathcal{D}_{\zeta\zeta}\mathfrak{u}(\zeta, \varrho) + \mathcal{D}_{\zeta\zeta\zeta\zeta}\mathfrak{u}(\zeta, \varrho) = 0, \tag{13}$$

subject to the initial condition:

$$\mathfrak{u}(\zeta,0)=a_1+\frac{15}{19}\sqrt{\frac{11}{19}}\left(-9\tanh[a_2(\zeta-a_3)]+11\tanh^3[a_2(\zeta-a_3)]\right), \tag{14}$$

Where a_1, a_2 and, a_3 are constants. The exact analytical solution is known and takes the form: [60]:

$$\mathfrak{u}(\zeta,\varrho)=a_1+\frac{15}{19}\sqrt{\frac{11}{19}}\left(-9\tanh[a_2(\zeta-a_1\varrho-a_3)]+11\tanh^3[a_2(\zeta-a_1\varrho-a_3)]\right).$$

Taking the LT to both sides of the equation (13) gives:

$$\mathcal{L}\left[\mathcal{D}_\varrho^\alpha\mathfrak{u}(\zeta,\varrho)\right]+\mathcal{L}\left[\mathfrak{u}(\zeta,\varrho)\mathcal{D}_\zeta\mathfrak{u}(\zeta,\varrho)\right]+\mathcal{L}\left[\mathcal{D}_{\zeta\zeta}\mathfrak{u}(\zeta,\varrho)\right]+\mathcal{L}\left[\mathcal{D}_{\zeta\zeta\zeta\zeta}\mathfrak{u}(\zeta,\varrho)\right]=0.$$

Here, $\mathcal{L}\left[\mathcal{D}_\varrho^\alpha\mathfrak{u}(\zeta,\varrho)\right]$ varies according to the definition of the fractional derivative, as shown in Table 1. After isolating $\mathcal{U}(\zeta,\mathfrak{s})$ and performing the inverse LT, we obtain:

$$\mathfrak{u}(\zeta,\varrho)=a_1+\frac{15}{19}\sqrt{\frac{11}{19}}\left(-9\tanh[a_2(\zeta-a_3)]+11\tanh^3[a_2(\zeta-a_3)]\right)-\mathcal{L}^{-1}\Big[\mathcal{F}(\mathfrak{s})\cdot\mathcal{L}\Big[\mathfrak{u}(\zeta,\varrho)\mathcal{D}_\zeta\mathfrak{u}(\zeta,\varrho)+\mathcal{D}_{\zeta\zeta}\mathfrak{u}(\zeta,\varrho)+\mathcal{D}_{\zeta\zeta\zeta\zeta}\mathfrak{u}(\zeta,\varrho)\Big]\Big], \tag{15}$$

Where $\mathcal{F}(\mathfrak{s})$ is an auxilary function that depends on the type of fractional derivative used and is given in Table (2).

Now, considering the solution $\mathfrak{u}(\zeta,\varrho)$ as an infinite series representation, expressed as:

$$\mathfrak{u}(\zeta,\varrho)=\sum_{n=0}^{\infty}\mathfrak{u}_n(\zeta,\varrho), \tag{16}$$

And the nonlinear term in the equation, $\mathfrak{u}(\zeta,\varrho)\mathcal{D}_\zeta\mathfrak{u}(\zeta,\varrho))$, are expressed as an infinite series of Adomian polynomials, defined as:

$$\mathfrak{u}(\zeta,\varrho)\mathcal{D}_\zeta\mathfrak{u}(\zeta,\varrho)=\sum_{n=0}^{\infty}\mathscr{A}_n(\zeta,\varrho), \tag{17}$$

Where:

$$\mathscr{A}_n(\zeta,\varrho)=\frac{1}{n!}\frac{d^n}{d\chi^n}\left[\left(\sum_{k=0}^{n}\chi^k\mathfrak{u}_k(\zeta,\varrho)\right)\mathcal{D}_\zeta\left(\sum_{k=0}^{n}\chi^k\mathfrak{u}_k(\zeta,\varrho)\right)\right]_{\chi=0}.$$

Inserting equations (16) and (17) into equation (15), we get:

$$\begin{cases}\mathfrak{u}_0(\zeta,\varrho)=a_1+\frac{15}{19}\sqrt{\frac{11}{19}}\left(-9\tanh[a_2(\zeta-a_3)]+11\tanh^3[a_2(\zeta-a_3)]\right)\\ \mathfrak{u}_{n+1}(\zeta,\varrho)=-\mathcal{L}^{-1}\left[\mathcal{F}(\mathfrak{s})\cdot\mathcal{L}\left[\mathscr{A}_n\left[\mathfrak{u}_n(\zeta,\varrho)\right]+\mathcal{D}_{\zeta\zeta}\mathfrak{u}_n(\zeta,\varrho)+\mathcal{D}_{\zeta\zeta\zeta\zeta}\mathfrak{u}_n(\zeta,\varrho)\right]\right]\end{cases}$$

By employing the Caputo derivative, the decomposition series begins with the following terms:

$$\mathfrak{u}_0(\zeta,\varrho)=a_1+\frac{15}{19}\sqrt{\frac{11}{19}}\left(-9\tanh[a_2(\zeta-a_3)]+11\tanh^3[a_2(\zeta-a_3)]\right).$$

$$\mathfrak{u}_1(\zeta,\varrho)=\frac{2475\,\varrho^\alpha\left(-7+4\cosh\left(\sqrt{\frac{11}{19}}(25+\zeta)\right)\right)\operatorname{sech}^4\left(\frac{1}{2}\sqrt{\frac{11}{19}}(25+\zeta)\right)}{722\,\Gamma(1+\alpha)}.$$

$$\mathfrak{u}_2(\zeta,\varrho)=\frac{12375\sqrt{\frac{11}{19}}\varrho^{2\alpha}\left(-9+2\cosh\left(\sqrt{\frac{11}{19}}(25+\zeta)\right)\right)\operatorname{sech}^4\left(\frac{1}{2}\sqrt{\frac{11}{19}}(25+\zeta)\right)\tanh\left(\frac{1}{2}\sqrt{\frac{11}{19}}(25+\zeta)\right)}{361\,\Gamma(1+2\alpha)}.$$

Hence, the L-ADM$_C$ solution to the IVP (13)–(14) takes the form:

$$\begin{aligned}\mathrm{u}(\zeta,\varrho) = {} & \frac{5\,\mathrm{sech}^4\left(\frac{1}{2}\sqrt{\frac{11}{19}}(25+\zeta)\right)}{54872}\left(\frac{37620\varrho^{\alpha}}{\Gamma(1+\alpha)}\left(-7+4\cosh\left(\sqrt{\frac{11}{19}}(25+\zeta)\right)\right)-\frac{19800\sqrt{209}\varrho^{2\alpha}\,\mathrm{sech}\left(\frac{1}{2}\sqrt{\frac{11}{19}}(25+\zeta)\right)}{\Gamma(1+2\alpha)}\right.\\ & \left.\left(-10\sinh\left(\frac{1}{2}\sqrt{\frac{11}{19}}(25+\zeta)\right)+\sinh\left(\frac{3}{2}\sqrt{\frac{11}{19}}(25+\zeta)\right)\right)-2280\sqrt{209}\sinh\left(\sqrt{\frac{11}{19}}(\zeta+25)\right)+20577\right.\\ & \left.+114\sqrt{209}\sinh\left(2\sqrt{\frac{11}{19}}(\zeta+25)\right)+27436\cosh\left(\sqrt{\frac{11}{19}}(\zeta+25)\right)+6859\cosh\left(2\sqrt{\frac{11}{19}}(\zeta+25)\right)+\ldots\right.\end{aligned}$$

For the case of the Caputo Fabrizio derivative, the first few terms of the decomposition series are given by:

$$\mathrm{u}_0(\zeta,\varrho) = a_1+\frac{15}{19}\sqrt{\frac{11}{19}}\left(-9\tanh[a_2(\zeta-a_3)]+11\tanh^3[a_2(\zeta-a_3)]\right).$$

$$\mathrm{u}_1(\zeta,\varrho) = -\frac{-2475(\alpha(\varrho-1)+1)}{722}\,\mathrm{sech}^4\left(\frac{1}{2}\sqrt{\frac{11}{19}}(\zeta+25)\right)\left(4\cosh\left(\sqrt{\frac{11}{19}}(\zeta+25)\right)-7\right).$$

$$\mathrm{u}_2(\zeta,\varrho) = -\frac{(12375)\left(\alpha^2\left(\varrho^2-4\varrho+2\right)+4\alpha(\varrho-1)+2\right)}{722}\sqrt{\frac{11}{19}}\,\mathrm{sech}^5\left(\frac{1}{2}\sqrt{\frac{11}{19}}(\zeta+25)\right)\left(\sinh\left(\frac{3}{2}\sqrt{\frac{11}{19}}(\zeta+25)\right)-10\sinh\left(\frac{1}{2}\sqrt{\frac{11}{19}}(\zeta+25)\right)\right).$$

Consequently, the L-ADM$_{CF}$ solution to the IVP (13)–(14) can be expressed as shown in Table 4 and Table 5:

$$\begin{aligned}\mathrm{u}(\zeta,\varrho) = {} & \frac{5}{109744}\,\mathrm{sech}^5\left(\frac{1}{2}\sqrt{\frac{11}{19}}(\zeta+25)\right)\left(-19800\sqrt{209}\alpha^2\varrho^2\sinh\left(\frac{3}{2}\sqrt{\frac{11}{19}}(\zeta+25)\right)+198000\sqrt{209}\alpha^2\varrho^2\sinh\left(\frac{1}{2}\sqrt{\frac{11}{19}}(\zeta+25)\right)\right.\\ & -792000\sqrt{209}\alpha^2\varrho\sinh\left(\frac{1}{2}\sqrt{\frac{11}{19}}(\zeta+25)\right)+79200\sqrt{209}\alpha^2\varrho\sinh\left(\frac{3}{2}\sqrt{\frac{11}{19}}(\zeta+25)\right)-79200\sqrt{209}\alpha\varrho\sinh\left(\frac{3}{2}\sqrt{\frac{11}{19}}(\zeta+25)\right)\\ & +792000\sqrt{209}\alpha\varrho\sinh\left(\frac{1}{2}\sqrt{\frac{11}{19}}(\zeta+25)\right)+190(1980\alpha(\varrho-1)+2341)\cosh\left(\frac{1}{2}\sqrt{\frac{11}{19}}(\zeta+25)\right)-95(1584\alpha(\varrho-1)+1223)\\ & \times\cosh\left(\frac{3}{2}\sqrt{\frac{11}{19}}(\zeta+25)\right)-39600\sqrt{209}\alpha^2\sinh\left(\frac{3}{2}\sqrt{\frac{11}{19}}(\zeta+25)\right)+396000\sqrt{209}\alpha^2\sinh\left(\frac{1}{2}\sqrt{\frac{11}{19}}(\zeta+25)\right)-792000\sqrt{209}\alpha\\ & \times\sinh\left(\frac{1}{2}\sqrt{\frac{11}{19}}(\zeta+25)\right)+79200\sqrt{209}\alpha\sinh\left(\frac{3}{2}\sqrt{\frac{11}{19}}(\zeta+25)\right)-41766\sqrt{209}\sinh\left(\frac{3}{2}\sqrt{\frac{11}{19}}(\zeta+25)\right)+393720\sqrt{209}\\ & \left.\times\sinh\left(\frac{1}{2}\sqrt{\frac{11}{19}}(\zeta+25)\right)+114\sqrt{209}\sinh\left(\frac{5}{2}\sqrt{\frac{11}{19}}(\zeta+25)\right)+6859\cosh\left(\frac{5}{2}\sqrt{\frac{11}{19}}(\zeta+25)\right)\right)+\ldots\end{aligned}$$

The decomposition associated with the Atangana–Baleanu derivative in the Caputo sense yields the following terms:

$$\mathrm{u}_0(\zeta,\varrho) = a_1+\frac{15}{19}\sqrt{\frac{11}{19}}\left(-9\tanh[a_2(\zeta-a_3)]+11\tanh^3[a_2(\zeta-a_3)]\right).$$

$$\mathrm{u}_1(\zeta,\varrho) = \frac{2475\left(\alpha\varrho^{\alpha}-(\alpha-1)\Gamma(\alpha+1)\right)}{722\Gamma(\alpha+1)}\,\mathrm{sech}^4\left(\frac{1}{2}\sqrt{\frac{11}{19}}(\zeta+25)\right)\left(4\cosh\left(\sqrt{\frac{11}{19}}(\zeta+25)\right)-7\right).$$

$$\mathrm{u}_2(\zeta,\varrho) = -\frac{12375\left(\Gamma(\alpha+1)\left((\alpha-1)^2\Gamma(2\alpha+1)+\alpha^2\varrho^{2\alpha}\right)-2(\alpha-1)\alpha\Gamma(2\alpha+1)\varrho^{\alpha}\right)}{361\Gamma(\alpha+1)\Gamma(2\alpha+1)}\,\mathrm{sech}^5\left(\frac{1}{2}\sqrt{\frac{11}{19}}(\zeta+25)\right)\times\sqrt{\frac{11}{19}}\left(\sinh\left(\frac{3}{2}\sqrt{\frac{11}{19}}(\zeta+25)\right)-10\sinh\left(\frac{1}{2}\sqrt{\frac{11}{19}}(\zeta+25)\right)\right).$$

Therfore, the corresponding L-ADM$_{ABC}$ solution to the IVP (13)-(14) is given by:

$$\begin{aligned}\mathrm{u}(\zeta,\varrho) = {} & \frac{5}{109744\Gamma(\alpha+1)\Gamma(2\alpha+1)}\,\mathrm{sech}^5\left(\frac{1}{2}\sqrt{\frac{11}{19}}(\zeta+25)\right)\left(\Gamma(2\alpha+1)\left(3960\alpha\varrho^{\alpha}\left(20\sqrt{209}(\alpha-1)\left(\sinh\left(\frac{3}{2}\sqrt{\frac{11}{19}}(\zeta+25)\right)\right.\right.\right.\right.\\ & \left.\left.\left.\left.-10\sinh\left(\frac{1}{2}\sqrt{\frac{11}{19}}(\zeta+25)\right)\right)+95\cosh\left(\frac{1}{2}\sqrt{\frac{11}{19}}(\zeta+25)\right)-38\cosh\left(\frac{3}{2}\sqrt{\frac{11}{19}}(\zeta+25)\right)\right)+\Gamma(\alpha+1)\left(-39600\sqrt{209}\alpha^2\right.\right.\right.\\ & \left.\left.\left.\times\sinh\left(\frac{3}{2}\sqrt{\frac{11}{19}}(\zeta+25)\right)+396000\sqrt{209}\alpha^2\sinh\left(\frac{1}{2}\sqrt{\frac{11}{19}}(\zeta+25)\right)-792000\sqrt{209}\alpha\sinh\left(\frac{1}{2}\sqrt{\frac{11}{19}}(\zeta+25)\right)+79200\sqrt{209}\alpha\right.\right.\right.\\ & \left.\left.\left.\times\sinh\left(\frac{3}{2}\sqrt{\frac{11}{19}}(\zeta+25)\right)-190(1980\alpha-2341)\cosh\left(\frac{1}{2}\sqrt{\frac{11}{19}}(\zeta+25)\right)+95(1584\alpha-1223)\cosh\left(\frac{3}{2}\sqrt{\frac{11}{19}}(\zeta+25)\right)-41766\sqrt{209}\right.\right.\right.\\ & \left.\left.\left.\times\sinh\left(\frac{3}{2}\sqrt{\frac{11}{19}}(\zeta+25)\right)+393720\sqrt{209}\sinh\left(\frac{1}{2}\sqrt{\frac{11}{19}}(\zeta+25)\right)+114\sqrt{209}\sinh\left(\frac{5}{2}\sqrt{\frac{11}{19}}(\zeta+25)\right)+6859\cosh\left(\frac{5}{2}\sqrt{\frac{11}{19}}(\zeta+25)\right)\right)\right)\right.\\ & \left.-39600\sqrt{209}\alpha^2\Gamma(\alpha+1)\varrho^{2\alpha}\left(\sinh\left(\frac{3}{2}\sqrt{\frac{11}{19}}(\zeta+25)\right)-10\sinh\left(\frac{1}{2}\sqrt{\frac{11}{19}}(\zeta+25)\right)\right)\right)+\ldots\end{aligned}$$

ISSN 2775-2658 International Journal of Robotics and Control Systems
Vol. 6, No. 1, 2026, pp. 793-818

Table 4. Absolute errors of the third-order approximations obtained by L-ADM$_C$, L-ADM$_{CF}$, L-ADM$_{ABC}$, and NTDM [60] for $\alpha = 1, 0.6, 0.4$, with $a_1 = \frac{3}{4}$, $a_2 = \frac{\sqrt{11}}{2\sqrt{19}}$, and $a_3 = -25$ in Application 1

		$\alpha = 0.4$				$\alpha = 0.6$				$\alpha = 1$	
ϱ	ζ	L-ADM$_C$	L-ADM$_{CF}$	L-ADM$_{ABC}$	NTDM	L-ADM$_C$	L-ADM$_{CF}$	L-ADM$_{ABC}$	NTDM	L-ADM$_C$	NTDM
	0.2	7.07×10^{-9}	2.82×10^{-8}	4.53×10^{-8}	1.16×10^{-6}	2.91×10^{-9}	7.53×10^{-9}	1.99×10^{-8}	8.54×10^{-7}	7.53×10^{-9}	6.87×10^{-8}
	0.4	6.07×10^{-9}	2.42×10^{-8}	3.89×10^{-8}	1.00×10^{-6}	2.5×10^{-9}	6.46×10^{-9}	1.71×10^{-8}	7.39×10^{-7}	6.46×10^{-9}	6.45×10^{-8}
0.1	0.6	5.22×10^{-9}	2.08×10^{-8}	2.34×10^{-8}	8.58×10^{-7}	2.14×10^{-9}	5.55×10^{-9}	1.47×10^{-8}	6.31×10^{-7}	5.55×10^{-9}	5.21×10^{-8}
	0.8	4.48×10^{-9}	1.78×10^{-8}	2.87×10^{-8}	7.38×10^{-7}	1.84×10^{-9}	4.77×10^{-9}	1.26×10^{-8}	5.43×10^{-7}	4.77×10^{-9}	4.60×10^{-8}
	1.0	3.85×10^{-9}	1.53×10^{-8}	2.46×10^{-8}	6.33×10^{-7}	1.58×10^{-9}	4.1×10^{-9}	1.08×10^{-8}	4.66×10^{-7}	4.1×10^{-9}	3.88×10^{-8}
	0.2	9.78×10^{-9}	2.42×10^{-8}	4.47×10^{-8}	1.12×10^{-6}	4.78×10^{-9}	1.46×10^{-8}	2.00×10^{-8}	8.69×10^{-7}	1.46×10^{-8}	1.19×10^{-7}
	0.4	8.40×10^{-9}	2.08×10^{-8}	3.84×10^{-8}	9.58×10^{-7}	4.1×10^{-9}	1.26×10^{-8}	1.72×10^{-8}	7.46×10^{-7}	1.26×10^{-8}	1.02×10^{-7}
0.2	0.6	7.21×10^{-9}	1.78×10^{-8}	3.3×10^{-8}	8.22×10^{-7}	3.52×10^{-9}	1.08×10^{-8}	1.48×10^{-8}	6.40×10^{-7}	1.08×10^{-8}	8.72×10^{-8}
	0.8	6.20×10^{-9}	1.53×10^{-8}	2.83×10^{-8}	7.07×10^{-7}	3.03×10^{-9}	9.27×10^{-9}	1.27×10^{-8}	5.51×10^{-7}	9.27×10^{-9}	7.59×10^{-8}
	1.0	5.32×10^{-9}	1.32×10^{-8}	2.43×10^{-8}	6.08×10^{-7}	2.6×10^{-9}	7.96×10^{-9}	1.09×10^{-8}	4.73×10^{-7}	7.96×10^{-9}	6.57×10^{-8}

Table 5. Absolute errors of the third-order approximations obtained by L-ADM$_C$, L-ADM$_{CF}$, L-ADM$_{ABC}$, and q-HATM [61] for $\alpha = 1, 0.9, 0.6$, with $a_1 = 5$, $a_2 = \frac{\sqrt{11}}{2\sqrt{19}}$, and $a_3 = -25$ in Application 1

		$\alpha = 0.6$				$\alpha = 0.9$				$\alpha = 1$	
ζ	ϱ	L-ADM$_C$	L-ADM$_{CF}$	L-ADM$_{ABC}$	q-HATM	L-ADM$_C$	L-ADM$_{CF}$	L-ADM$_{ABC}$	q-HATM	L-ADM$_C$	q-HATM
	0.2	1.76×10^{-7}	3.43×10^{-7}	5.43×10^{-7}	2.10×10^{-5}	1.96×10^{-8}	6.09×10^{-8}	9.18×10^{-8}	2.67×10^{-6}	6.63×10^{-9}	2.80×10^{-8}
	0.4	2.4×10^{-7}	3.22×10^{-7}	5.75×10^{-7}	4.16×10^{-5}	1.38×10^{-8}	2.17×10^{-8}	7.66×10^{-8}	5.50×10^{-6}	6.65×10^{-8}	4.95×10^{-7}
1	0.6	1.07×10^{-7}	1.12×10^{-7}	3.84×10^{-7}	6.18×10^{-5}	2.11×10^{-7}	1.88×10^{-7}	1.13×10^{-7}	7.47×10^{-6}	2.89×10^{-7}	2.78×10^{-6}
	0.8	4.58×10^{-7}	5.23×10^{-7}	2.58×10^{-7}	7.68×10^{-5}	8.1×10^{-7}	8.03×10^{-7}	7.12×10^{-7}	5.46×10^{-6}	9.08×10^{-7}	9.83×10^{-6}
	1.0	1.96×10^{-6}	2.08×10^{-6}	1.85×10^{-6}	7.98×10^{-5}	2.31×10^{-6}	2.32×10^{-6}	2.22×10^{-6}	6.17×10^{-6}	2.43×10^{-6}	2.70×10^{-5}
	0.2	8.39×10^{-9}	1.64×10^{-8}	2.57×10^{-8}	3.37×10^{-6}	9.35×10^{-10}	2.9×10^{-9}	4.38×10^{-9}	4.57×10^{-9}	3.16×10^{-10}	4.57×10^{-9}
	0.4	1.14×10^{-8}	1.54×10^{-8}	2.74×10^{-8}	6.70×10^{-6}	6.58×10^{-10}	1.04×10^{-9}	3.65×10^{-9}	8.09×10^{-8}	3.17×10^{-9}	8.09×10^{-8}
5	0.6	5.09×10^{-8}	5.32×10^{-8}	1.83×10^{-8}	9.96×10^{-6}	1.01×10^{-8}	8.97×10^{-8}	5.39×10^{-8}	4.55×10^{-7}	1.38×10^{-8}	4.55×10^{-7}
	0.8	1.38×10^{-8}	2.5×10^{-8}	1.38×10^{-8}	1.24×10^{-5}	3.86×10^{-8}	3.83×10^{-8}	3.39×10^{-8}	3.61×10^{-7}	4.33×10^{-8}	3.61×10^{-7}
	1.0	9.33×10^{-8}	9.93×10^{-8}	8.8×10^{-8}	1.28×10^{-5}	1.1×10^{-7}	1.11×10^{-7}	1.06×10^{-7}	4.43×10^{-7}	1.16×10^{-7}	4.43×10^{-7}

Fig. 2, Fig. 3, Fig. 4 and Table 4, Table 5 present the numerical and graphical results of **Application 1** for different values of the fractional order α. Fig. 2 shows a close agreement between the exact and approximate solutions obtained from the three variants of the L-ADM.

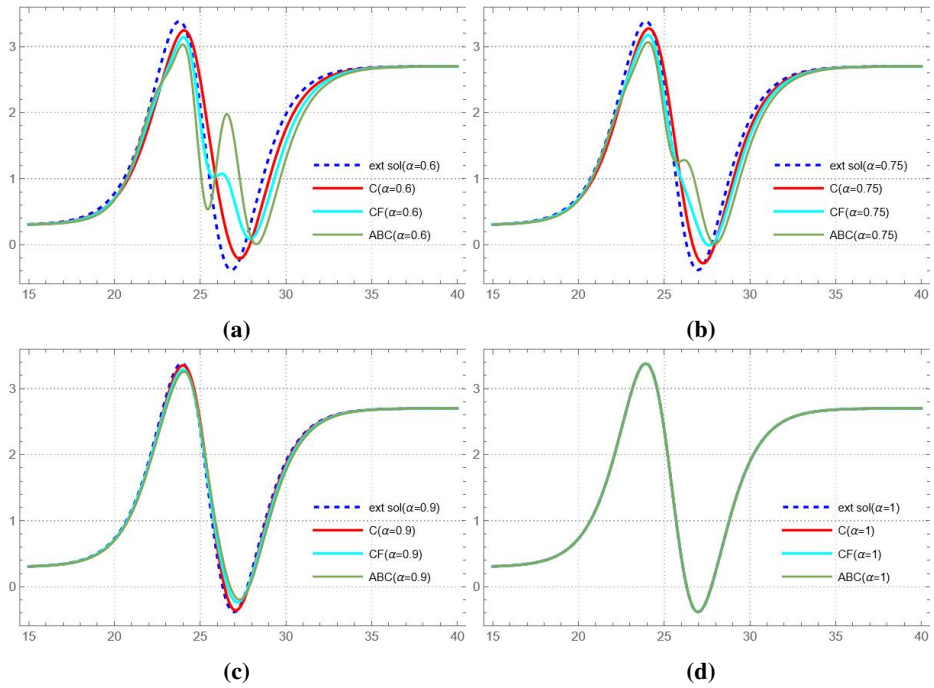

Fig. 2. 2D plots of the exact and third-order approximate solutions obtained by L-ADM$_C$, L-ADM$_{CF}$, and L-ADM$_{ABC}$ for Application 1 at various fractional orders α, with $15 \leq \zeta \leq 40$ and $\varrho = 0.4$, where $a_1 = \frac{3}{2}$, $a_2 = \frac{\sqrt{11}}{2\sqrt{19}}$, and $a_3 = 25$

As α decreases from 1 toward fractional values, the wave amplitude becomes smaller and the solution profile smoother, revealing the memory-induced damping typical of fractional-order systems. This attenuation indicates that smaller α values enhance diffusion and slow down temporal evolution. Among the three fractional derivatives, the Caputo produces the most regular and stable waveforms, followed by Caputo-Fabrizio, while Atangana-Baleanu (Caputo sense) exhibits the most pronounced flattening of the peaks.

This ordering corresponds to the strength and nature of their memory kernels: the singular power-law kernel of Caputo better preserves local dynamics, whereas the exponential (CF) and Mittag-Leffler (ABC) kernels introduce stronger smoothing and long-range diffusion. The 3D surfaces in Fig. 3 further confirm these observations. For all values of α, the approximate surfaces generated by the three L-ADM formulations almost coincide with the exact analytical surface, demonstrating the high precision of the method.

When α is reduced, the surface amplitude decreases and the surface changes more smoothly over time, showing the stronger damping effect of the fractional order. The Caputo variant again provides the most coherent and physically realistic surface, with smooth transitions and minimal deviation from the exact one. The Caputo-Fabrizio and Atangana-Baleanu (Caputo sense) forms yield slightly more diffusive and flattened surfaces because their non-singular kernels reduce the short-term memory effect.

Overall, variation of α controls the degree of wave damping and smoothness: higher α values retain sharper oscillations, while lower α values lead to stable, diffusive wave patterns. Fig. 4 illustrates the absolute error distribution across the spatial domain.

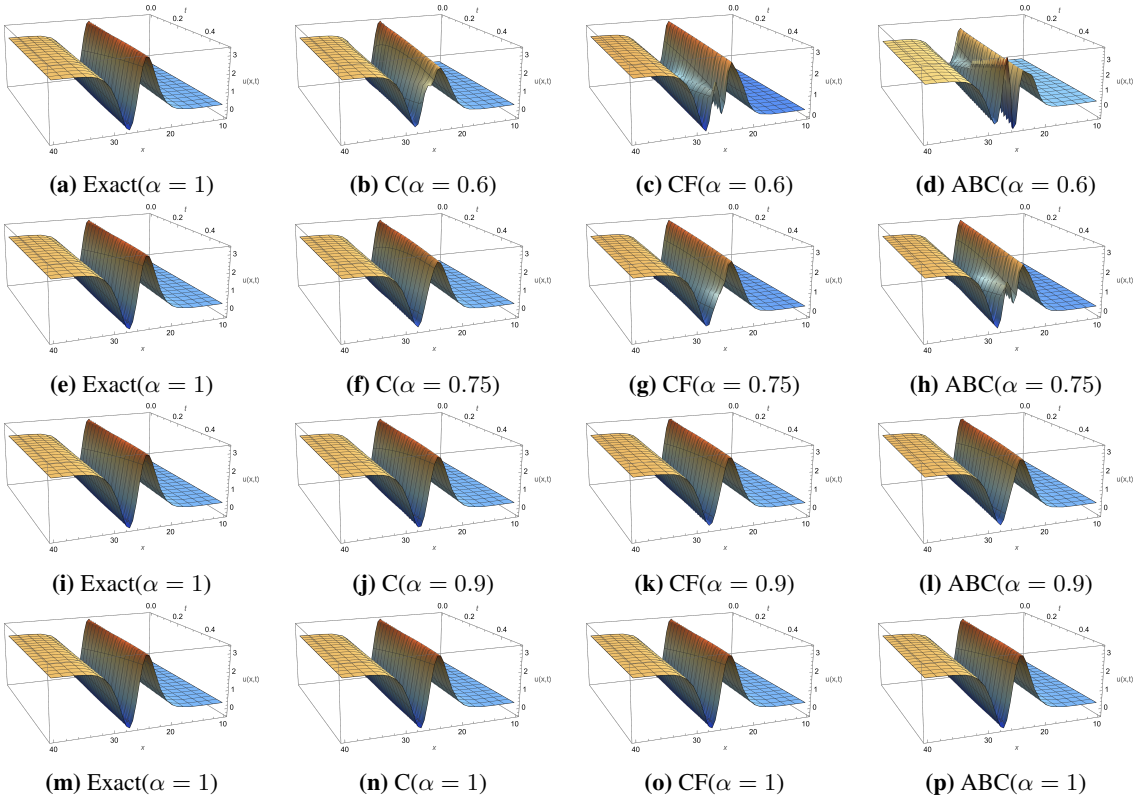

(a) Exact($\alpha = 1$) **(b)** C($\alpha = 0.6$) **(c)** CF($\alpha = 0.6$) **(d)** ABC($\alpha = 0.6$)

(e) Exact($\alpha = 1$) **(f)** C($\alpha = 0.75$) **(g)** CF($\alpha = 0.75$) **(h)** ABC($\alpha = 0.75$)

(i) Exact($\alpha = 1$) **(j)** C($\alpha = 0.9$) **(k)** CF($\alpha = 0.9$) **(l)** ABC($\alpha = 0.9$)

(m) Exact($\alpha = 1$) **(n)** C($\alpha = 1$) **(o)** CF($\alpha = 1$) **(p)** ABC($\alpha = 1$)

Fig. 3. 3D plots of the exact and third-order approximate solutions obtained by L-ADM$_C$, L-ADM$_{CF}$, and L-ADM$_{ABC}$ Solutions for Application 1 at Different values of α, with $10 \leq \zeta \leq 40$ and $0 \leq \rho \leq 0.5$, where $a_1 = \frac{3}{2}$, $a_2 = \frac{\sqrt{11}}{2\sqrt{19}}$, and $a_3 = 25$

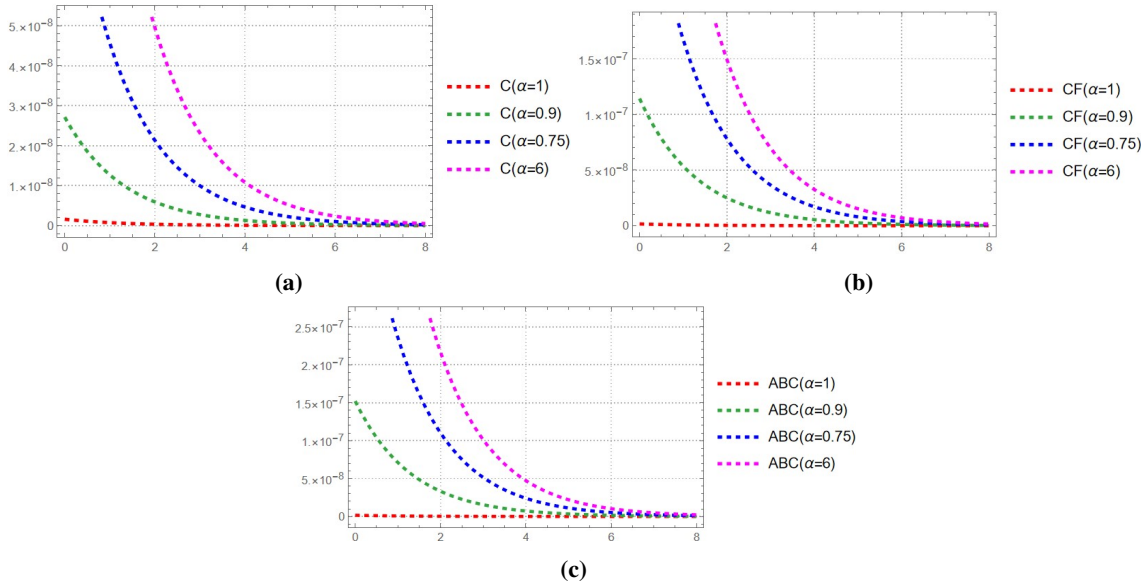

(a) **(b)**

(c)

Fig. 4. 2D graphs of the absolute errors of the third-order approximations for L-ADM$_C$, L-ADM$_{CF}$, and L-ADM$_{ABC}$ in Application 1, at different values of α, for $0 \leq \zeta \leq 8$, and with $\varrho = 0.1$, where $a_1 = 5$, $a_2 = \frac{\sqrt{11}}{2\sqrt{19}}$, and $a_3 = -25$

The errors remain extremely small in all cases, confirming the numerical stability and rapid convergence of L-ADM. A slight increase in error with decreasing α is observed, reflecting the growing non-locality of the fractional operator. Quantitatively, the Caputo derivative produces the smallest overall errors, while the Caputo-Fabrizio and Atangana-Baleanu (Caputo sense) derivatives show slightly higher but smoother error profiles—consistent with their more diffusive nature. These results demonstrate that all three versions of L-ADM are robust, but the Caputo definition provides the highest accuracy.

Table 4 reports a quantitative comparison of the approximations for the three L-ADM variants and the new transform decomposition method (NTDM) [60]. Across all fractional orders, L-ADM yields considerably smaller absolute errors than NTDM, confirming its superior convergence and computational efficiency. Again, the Caputo formulation achieves the highest precision, while the Caputo-Fabrizio and Atangana-Baleanu (Caputo sense) versions maintain good accuracy with smoother numerical behavior. These results confirm that the singular kernel of Caputo enhances local accuracy, whereas the exponential and Mittag-Leffler kernels trade accuracy for smoothness.

Table 5 extends the comparison to include the q-HATM approach. For all α values, the errors of L-ADM remain on the order of 10^{-7} or smaller, which demonstrates rapid series convergence and high numerical efficiency. Although the absolute error slightly increases as α decreases, the method preserves excellent precision in every case. The results show that the L-ADM in the Caputo sense offers the best accuracy, while Caputo-Fabrizio and Atangana-Baleanu (Caputo sense) still provide smooth and stable approximations. In addition, L-ADM outperforms NTDM and q-HATM in both accuracy and computational simplicity, showing its advantage for nonlinear fractional problems.

5.2. Application 2

Now, we focus on the fractional KS equation, subject to $\sigma = 1$, $\eta = 4$ and $\mu = 1$, given by:

$$\mathcal{D}_{\varrho}^{\alpha}\mathfrak{u}(\zeta,\varrho) + \mathfrak{u}(\zeta,\varrho)\mathcal{D}_{\zeta}\mathfrak{u}(\zeta,\varrho) + \mathcal{D}_{\zeta\zeta}\mathfrak{u}(\zeta,\varrho) + 4\mathcal{D}_{\zeta\zeta\zeta}\mathfrak{u}(\zeta,\varrho) + \mathcal{D}_{\zeta\zeta\zeta\zeta}\mathfrak{u}(\zeta,\varrho) = 0, \tag{18}$$

under the initial condition:

$$\mathfrak{u}(\zeta,0) = a_1 + 9 - 15\left(\tanh[a_2(\zeta - a_3)] + \tanh^2[a_2(\zeta - a_3)] - \tanh^3[a_2(\zeta - a_3)]\right). \tag{19}$$

The exact solution of the given IVP is expressed as follows [60]:

$$\mathfrak{u}(\zeta,\varrho) = a_1 + 9 - 15\left(\tanh[a_2(\zeta - a_1\varrho - a_3)] + \tanh^2[a_2(\zeta - a_1\varrho - a_3)] - \tanh^3[a_2(\zeta - a_1\varrho - a_3)]\right).$$

By applying the LT to both sides of the equation (18), we obtain:

$$\mathcal{L}\left[\mathcal{D}_{\varrho}^{\alpha}\mathfrak{u}(\zeta,\varrho)\right] + \mathcal{L}\left[\mathfrak{u}(\zeta,\varrho)\mathcal{D}_{\zeta}\mathfrak{u}(\zeta,\varrho)\right] + \mathcal{L}\left[\mathcal{D}_{\zeta\zeta}\mathfrak{u}(\zeta,\varrho)\right] + 4\mathcal{L}\left[\mathcal{D}_{\zeta\zeta\zeta}\mathfrak{u}(\zeta,\varrho)\right] + \mathcal{L}\left[\mathcal{D}_{\zeta\zeta\zeta\zeta}\mathfrak{u}(\zeta,\varrho)\right] = 0$$

Employing the LT identities associated with the different definitions of the fractional derivatives (see Table (1)), and after rearranging the expression to isolate $\mathcal{U}(\zeta,\mathfrak{s})$ and performing the inverse LT, we arrive at:

$$\begin{aligned}\mathfrak{u}(\zeta,\varrho) = {} & a_1 + 9 - 15\left(\tanh[a_2(\zeta - a_3)] + \tanh^2[a_2(\zeta - a_3)] - \tanh^3[a_2(\zeta - a_3)]\right) \\ & - \mathcal{L}^{-1}\left[\mathcal{F}(\mathfrak{s})\cdot\mathcal{L}\left[\mathfrak{u}(\zeta,\varrho)\mathcal{D}_{\zeta}\mathfrak{u}(\zeta,\varrho) + \mathcal{D}_{\zeta\zeta}\mathfrak{u}(\zeta,\varrho) + 4\mathcal{D}_{\zeta\zeta\zeta}\mathfrak{u}(\zeta,\varrho) + \mathcal{D}_{\zeta\zeta\zeta\zeta}\mathfrak{u}(\zeta,\varrho)\right]\right],\end{aligned} \tag{20}$$

Here, $\mathcal{F}(\mathfrak{s})$ depends on the chosen definition of the fractional derivative (see Table 2).

Now, considering the solution $\mathfrak{u}(\zeta,\varrho)$ as an infinite series representation, expressed as:

$$\mathfrak{u}(\zeta,\varrho) = \sum_{n=0}^{\infty}\mathfrak{u}_n(\zeta,\varrho), \tag{21}$$

and the nonlinear term in the equation, $\mathfrak{u}(\zeta,\varrho)\mathcal{D}_\zeta\mathfrak{u}(\zeta,\varrho))$, are expressed as an infinite series of Adomian polynomials, defined as:

$$\mathfrak{u}(\zeta,\varrho)\mathcal{D}_\zeta\mathfrak{u}(\zeta,\varrho)=\sum_{n=0}^{\infty}\mathscr{A}_n(\zeta,\varrho), \tag{22}$$

Where:

$$\mathscr{A}_n(\zeta,\varrho)=\frac{1}{n!}\frac{d^n}{d\chi^n}\left[\left(\sum_{k=0}^{n}\chi^k\mathfrak{u}_k(\zeta,\varrho)\right)\mathcal{D}_\zeta\left(\sum_{k=0}^{n}\chi^k\mathfrak{u}_k(\zeta,\varrho)\right)\right]_{\chi=0}.$$

Inserting equations (21) and (22) in equation (20) , we get:

$$\begin{cases}\mathfrak{u}_0(\zeta,\varrho)=a_1+9-15\left(\tanh[a_2(x-a_3)]+\tanh^2[a_2(x-a_3)]-\tanh^3[a_2(x-a_3)]\right)\\ \mathfrak{u}_{n+1}(x,\varrho)=-\mathcal{L}^{-1}\left[\mathcal{F}(\mathfrak{s})\cdot\mathcal{L}\left[\mathscr{A}_n\left[\mathfrak{u}_n(\zeta,\varrho)\right]+\mathcal{D}_{\zeta\zeta}\mathfrak{u}_n(\zeta,\varrho)+4\mathcal{D}_{\zeta\zeta\zeta}\mathfrak{u}_n(\zeta,\varrho)+\mathcal{D}_{\zeta\zeta\zeta\zeta}\mathfrak{u}_n(\zeta,\varrho)\right]\right]\end{cases} \tag{23}$$

For the Caputo derivative, the first terms of the recurrence sequence are:

$$\mathfrak{u}_0(\zeta,\varrho)=a_1+9-15\left(\tanh[a_2(\zeta-a_3)]+\tanh^2[a_2(\zeta-a_3)]-\tanh^3[a_2(\zeta-a_3)]\right).$$

$$\mathfrak{u}_1(\zeta,\varrho)=\frac{360e^{13}\varrho^\alpha\left(\cosh\left(\frac{\zeta}{2}\right)-\sinh\left(\frac{\zeta}{2}\right)\right)}{\Gamma(\alpha+1)\left(\left(e^{13}-1\right)\sinh\left(\frac{\zeta}{2}\right)+\left(1+e^{13}\right)\cosh\left(\frac{\zeta}{2}\right)\right)^4}\left(\left(1+2e^{13}\right)\sinh\left(\frac{\zeta}{2}\right)+\left(2e^{13}-1\right)\cosh\left(\frac{\zeta}{2}\right)\right).$$

$$\mathfrak{u}_2(\zeta,\varrho)=\frac{1080e^{13}\varrho^{2\alpha}\left(\cosh\left(\frac{\zeta}{2}\right)-\sinh\left(\frac{\zeta}{2}\right)\right)}{\Gamma(2\alpha+1)\left(\left(e^{13}-1\right)\sinh\left(\frac{\zeta}{2}\right)+\left(1+e^{13}\right)\cosh\left(\frac{\zeta}{2}\right)\right)^5}\left(\left(4e^{26}-1\right)\sinh(\zeta)+\left(1+4e^{26}\right)\cosh(\zeta)-7e^{13}\right).$$

Hence, the L-ADM$_C$ solution corresponding to the IVP (18)-(19) can be written as:

$$\begin{aligned}\mathfrak{u}(\zeta,\varrho)=&\frac{3}{\Gamma(\alpha+1)\Gamma(2\alpha+1)\left(\left(e^{13}-1\right)\sinh\left(\frac{\zeta}{2}\right)+\left(1+e^{13}\right)\cosh\left(\frac{\zeta}{2}\right)\right)^5}\Bigg(120e^{13}\Gamma(2\alpha+1)\varrho^\alpha\left(\cosh\left(\frac{\zeta}{2}\right)-\sinh\left(\frac{\zeta}{2}\right)\right)\Bigg(2e^{26}\sinh(\zeta)\\&+\sinh(\zeta)+\left(2e^{26}-1\right)\cosh(\zeta)+e^{13}\Bigg)-\Gamma(\alpha+1)\Bigg(\Gamma(2\alpha+1)\Bigg(\left(e^{13}-1\right)\sinh\left(\frac{\zeta}{2}\right)+\left(1+e^{13}\right)\cosh\left(\frac{\zeta}{2}\right)\Bigg)^2\Bigg(e^{13}\left(3e^{13}-37\right)\\&\times\cosh\left(\frac{\zeta}{2}\right)+\left(1+e^{39}\right)\cosh\left(\frac{3\zeta}{2}\right)+\sinh\left(\frac{\zeta}{2}\right)\left(2\left(e^{39}-1\right)\cosh(\zeta)+e^{39}+3e^{26}+37e^{13}-1\right)\Bigg)-360e^{13}t^{2\alpha}\Bigg(\cosh\left(\frac{\zeta}{2}\right)\\&-\sinh\left(\frac{\zeta}{2}\right)\Bigg)\Bigg(\left(4e^{26}-1\right)\sinh(\zeta)+\left(1+4e^{26}\right)\cosh(\zeta)-7e^{13}\Bigg)\Bigg)\Bigg)+\ldots\end{aligned}$$

Proceeding with the Caputo–Fabrizio derivative, the initial terms of the recurrence sequence are expressed as:

$$\mathfrak{u}_0(\zeta,\varrho)=a_1+9-15\left(\tanh[a_2(\zeta-a_3)]+\tanh^2[a_2(\zeta-a_3)]-\tanh^3[a_2(\zeta-a_3)]\right).$$

$$\mathfrak{u}_1(\zeta,\varrho)=\frac{360e^{13}(\alpha(\varrho-1)+1)}{\left(\left(e^{13}-1\right)\sinh\left(\frac{\zeta}{2}\right)+\left(1+e^{13}\right)\cosh\left(\frac{\zeta}{2}\right)\right)^4}\left(\cosh\left(\frac{\zeta}{2}\right)-\sinh\left(\frac{\zeta}{2}\right)\right)\left(\left(1+2e^{13}\right)\sinh\left(\frac{\zeta}{2}\right)+\left(2e^{13}-1\right)\cosh\left(\frac{\zeta}{2}\right)\right).$$

$$\mathfrak{u}_2(\zeta,\varrho)=\frac{540e^{13}\left(\alpha^2\left(\varrho^2-4\varrho+2\right)+4\alpha(\varrho-1)+2\right)}{\left(\left(e^{13}-1\right)\sinh\left(\frac{\zeta}{2}\right)+\left(1+e^{13}\right)\cosh\left(\frac{\zeta}{2}\right)\right)^5}\left(\cosh\left(\frac{\zeta}{2}\right)-\sinh\left(\frac{\zeta}{2}\right)\right)\left(\left(4e^{26}-1\right)\sinh(\zeta)+\left(1+4e^{26}\right)\cosh(\zeta)-7e^{13}\right).$$

Therfore, the L-ADM$_{CF}$ solution to the IVP (18)-(19) is expressed as follows:

$$\begin{aligned}\mathfrak{u}(\zeta,\varrho)=-&\frac{3}{\left(\left(e^{13}-1\right)\sinh\left(\frac{\zeta}{2}\right)+\left(1+e^{13}\right)\cosh\left(\frac{\zeta}{2}\right)\right)^5}\Bigg(-720e^{39}\alpha^2\varrho^2\sinh\left(\frac{\zeta}{2}\right)-1260e^{26}\alpha^2\varrho^2\sinh\left(\frac{\zeta}{2}\right)+180e^{13}\alpha^2\varrho^2\sinh\left(\frac{3\zeta}{2}\right)\\&-10e^{26}\left(-126\alpha^2\left(\varrho^2-4t+2\right)+3e^{13}\left(24\alpha^2\left(\varrho^2-4\varrho+2\right)+104\alpha(\varrho-1)+57\right)-492\alpha(\varrho-1)-233\right)\cosh\left(\frac{\zeta}{2}\right)+5e^{13}\\&\times\left(-36\alpha^2\left(\varrho^2-4\varrho+2\right)-120\alpha(\varrho-1)+e^{39}-55\right)\cosh\left(\frac{3\zeta}{2}\right)+2880e^{39}\alpha^2\varrho\sinh\left(\frac{\zeta}{2}\right)+5040e^{26}\alpha^2\varrho\sinh\left(\frac{\zeta}{2}\right)-720e^{13}\alpha^2\varrho\sinh\left(\frac{3\zeta}{2}\right)\\&-3120e^{39}\alpha\varrho\sinh\left(\frac{\zeta}{2}\right)-4920e^{26}\alpha\varrho\sinh\left(\frac{\zeta}{2}\right)+600e^{13}\alpha\varrho\sinh\left(\frac{3\zeta}{2}\right)-1440e^{39}\alpha^2\sinh\left(\frac{\zeta}{2}\right)-2520e^{26}\alpha^2\sinh\left(\frac{\zeta}{2}\right)+360e^{13}\alpha^2\sinh\left(\frac{3\zeta}{2}\right)\\&+3120e^{39}\alpha\sinh\left(\frac{\zeta}{2}\right)+4920e^{26}\alpha\sinh\left(\frac{\zeta}{2}\right)-600e^{13}\alpha\sinh\left(\frac{3\zeta}{2}\right)-1710e^{39}\sinh\left(\frac{\zeta}{2}\right)-2330e^{26}\sinh\left(\frac{\zeta}{2}\right)+5e^{52}\sinh\left(\frac{3\zeta}{2}\right)\\&+275e^{13}\sinh\left(\frac{3\zeta}{2}\right)+e^{65}\sinh\left(\frac{5\zeta}{2}\right)-\sinh\left(\frac{5\zeta}{2}\right)+e^{65}\cosh\left(\frac{5\zeta}{2}\right)+\cosh\left(\frac{5\zeta}{2}\right)\Bigg)+\ldots\end{aligned}$$

For the Atangana–Baleanu derivative in the Caputo sense, the decomposition sequence yields shown in Table 6 and Table 7:

$$u_0(\zeta,\varrho) = a_1 + 9 - 15\left(\tanh[a_2(\zeta - a_3)] + \tanh^2[a_2(\zeta - a_3)] - \tanh^3[a_2(\zeta - a_3)]\right)$$

$$u_1(\zeta,\varrho) = \frac{360e^{13}\left(\alpha\varrho^{\alpha} - (\alpha-1)\Gamma(\alpha+1)\right)}{\Gamma(\alpha+1)\left((e^{13}-1)\sinh\left(\frac{\zeta}{2}\right) + (1+e^{13})\cosh\left(\frac{\zeta}{2}\right)\right)^4}\left(\cosh\left(\frac{\zeta}{2}\right) - \sinh\left(\frac{\zeta}{2}\right)\right)\left(\left(1+2e^{13}\right)\sinh\left(\frac{\zeta}{2}\right) + \left(2e^{13}-1\right)\cosh\left(\frac{\zeta}{2}\right)\right)$$

$$u_2(\zeta,\varrho) = \frac{1080e^{13}\left(\Gamma(\alpha+1)\left((\alpha-1)^2\Gamma(2\alpha+1) + \alpha^2\varrho^{2\alpha}\right) - 2(\alpha-1)\alpha\Gamma(2\alpha+1)\varrho^{\alpha}\right)}{\Gamma(\alpha+1)\Gamma(2\alpha+1)\left((e^{13}-1)\sinh\left(\frac{\zeta}{2}\right) + (1+e^{13})\cosh\left(\frac{\zeta}{2}\right)\right)^5}\left(\cosh\left(\frac{\zeta}{2}\right) - \sinh\left(\frac{\zeta}{2}\right)\right)$$
$$\times\left(\left(4e^{26}-1\right)\sinh(\zeta) + \left(1+4e^{26}\right)\cosh(\zeta) - 7e^{13}\right)$$

Accordingly, the L-ADM$_{ABC}$ solution to the IVP (18)-(19) takes the form shown in Fig. 5:

$$u(\zeta,\varrho) = -\frac{3}{\Gamma(\alpha+1)\Gamma(2\alpha+1)\left((e^{13}-1)\sinh\left(\frac{\zeta}{2}\right) + (1+e^{13})\cosh\left(\frac{\zeta}{2}\right)\right)^5}\Bigg(\Gamma(\alpha+1)\Bigg(\Gamma(2\alpha+1)\Bigg(-1440e^{39}\alpha^2\sinh\left(\frac{\zeta}{2}\right) - 2520e^{26}\alpha^2$$
$$\sinh\left(\frac{\zeta}{2}\right) + 360e^{13}\alpha^2 \times \sinh\left(\frac{3\zeta}{2}\right) - 10e^{26}\left(-252\alpha^2 + 3e^{13}\left(48\alpha^2 - 104\alpha + 57\right) + 492\alpha - 233\right)\cosh\left(\frac{\zeta}{2}\right) + 5e^{13}\Bigg(-72\alpha^2 + 120\alpha$$
$$+ e^{39} - 55\Bigg)\cosh\left(\frac{3\zeta}{2}\right) + 3120e^{39}\alpha\sinh\left(\frac{\zeta}{2}\right) + 4920e^{26}\alpha\sinh\left(\frac{\zeta}{2}\right) - 600e^{13}\alpha\sinh\left(\frac{3\zeta}{2}\right) - 1710e^{39}\sinh\left(\frac{\zeta}{2}\right) - 2330e^{26}\sinh\left(\frac{\zeta}{2}\right)$$
$$+ 5e^{52}\sinh\left(\frac{3\zeta}{2}\right) + 275e^{13}\sinh\left(\frac{3\zeta}{2}\right) + e^{65}\sinh\left(\frac{5\zeta}{2}\right) - \sinh\left(\frac{5\zeta}{2}\right) + e^{65}\cosh\left(\frac{5\zeta}{2}\right) + \cosh\left(\frac{5\zeta}{2}\right)\Bigg) - 360e^{13}\alpha^2\varrho^{2\alpha}\Bigg(\cosh\left(\frac{\zeta}{2}\right)$$
$$- \sinh\left(\frac{\zeta}{2}\right)\Bigg)\left(\left(4e^{26}-1\right)\sinh(\zeta) + \left(1+4e^{26}\right)\cosh(\zeta) - 7e^{13}\right)\Bigg) + 120e^{13}\alpha\Gamma(2\alpha+1)t^{\alpha}\left(\cosh\left(\frac{\zeta}{2}\right) - \sinh\left(\frac{\zeta}{2}\right)\right)\Big(e^{13}(41-42\alpha)$$
$$+ \left(-6\alpha + e^{26}(24\alpha - 26) + 5\right)\sinh(\zeta) + \left(6\alpha + e^{26}(24\alpha - 26) - 5\right)\cosh(\zeta)\Big)\Bigg) + \ldots$$

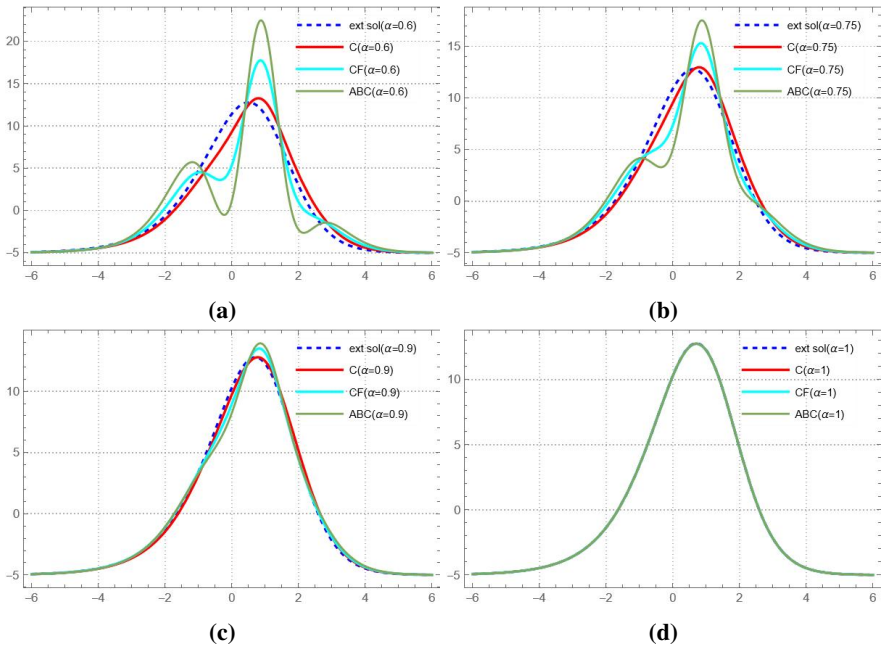

Fig. 5. 2D graphs of the exact third order approximate solutions and L-ADM$_C$, L-ADM$_{CF}$, and L-ADM$_{ABC}$ solutions for Application 2 at different values of α, with $-6 \le \zeta \le 6$, and for $\varrho = 0.4$, where $a_1 = 1$, $a_2 = \frac{1}{2}$, and $a_3 = 1$

ISSN 2775-2658 International Journal of Robotics and Control Systems
Vol. 6, No. 1, 2026, pp. 793-818

Table 6. Absolute errors of the exact and third-order approximate solutions obtained by L-ADM$_C$, L-ADM$_{CF}$, L-ADM$_{ABC}$ and NTDM [60] for $\alpha = 1, 0.6, 0.4$, with $a_1 = \frac{3}{4}$, $a_2 = \frac{1}{2}$, and $a_3 = -13$ in Application 2

		$\alpha = 0.4$				$\alpha = 0.6$				$\alpha = 1$	
ϱ	ζ	L-ADM$_C$	L-ADM$_{CF}$	L-ADM$_{ABC}$	NTDM	L-ADM$_C$	L-ADM$_{CF}$	L-ADM$_{ABC}$	NTDM	L-ADM$_C$	NTDM
	0.2	2.48×10^{-10}	6.9×10^{-10}	1.05×10^{-9}	7.60×10^{-7}	3.94×10^{-11}	3.21×10^{-10}	5.17×10^{-10}	7.10×10^{-8}	5.73×10^{-11}	1.1×10^{-8}
	0.4	1.66×10^{-10}	4.62×10^{-10}	7.02×10^{-10}	5.13×10^{-7}	2.64×10^{-11}	2.15×10^{-10}	3.47×10^{-10}	5.1×10^{-8}	3.84×10^{-11}	1.2×10^{-8}
0.1	0.6	1.12×10^{-10}	3.10×10^{-10}	4.71×10^{-10}	3.35×10^{-7}	1.77×10^{-11}	1.44×10^{-10}	2.32×10^{-10}	4.1×10^{-8}	2.57×10^{-11}	0.0×10^{-0}
	0.8	7.48×10^{-11}	2.08×10^{-10}	3.16×10^{-10}	2.31×10^{-7}	1.19×10^{-11}	9.68×10^{-11}	1.56×10^{-10}	3.8×10^{-8}	1.72×10^{-11}	1.0×10^{-9}
	1.0	5.01×10^{-11}	1.39×10^{-10}	2.12×10^{-10}	1.52×10^{-7}	7.96×10^{-12}	6.49×10^{-11}	1.04×10^{-10}	1.8×10^{-8}	1.16×10^{-11}	1.1×10^{-9}
	0.2	4.04×10^{-10}	7.05×10^{-10}	1.14×10^{-9}	5.49×10^{-7}	9.95×10^{-11}	3.43×10^{-10}	6.18×10^{-10}	5.1×10^{-8}	1.07×10^{-10}	1.4×10^{-8}
	0.4	2.71×10^{-10}	4.73×10^{-10}	7.61×10^{-10}	3.63×10^{-7}	6.67×10^{-11}	2.3×10^{-10}	4.14×10^{-10}	2.8×10^{-8}	7.16×10^{-11}	1.3×10^{-8}
0.2	0.6	1.82×10^{-10}	3.17×10^{-10}	5.1×10^{-10}	2.38×10^{-7}	4.47×10^{-11}	1.54×10^{-10}	2.78×10^{-10}	3.6×10^{-8}	4.80×10^{-11}	1.5×10^{-8}
	0.8	1.22×10^{-10}	2.12×10^{-10}	3.42×10^{-10}	1.70×10^{-7}	3.00×10^{-11}	1.03×10^{-10}	1.86×10^{-10}	3.1×10^{-8}	3.22×10^{-1}	1.1×10^{-8}
	1.0	8.16×10^{-11}	1.55×10^{-10}	2.29×10^{-10}	9.80×10^{-8}	2.01×10^{-11}	6.92×10^{-11}	1.25×10^{-10}	1.0×10^{-8}	2.16×10^{-11}	0.0×10^{0}

Table 7. Absolute errors of the exact and third-order approximate solutions obtained byL-ADM$_C$, L-ADM$_{CF}$, L-ADM$_{ABC}$ and q-HATM [61] for $\alpha = 1, 0.9, 0.6$, with $a_1 = 3$, $a_2 = \frac{1}{2}$, and $a_3 = -13$ in Application 2

		$\alpha = 0.6$				$\alpha = 0.9$				$\alpha = 1$	
ζ	ϱ	L-ADM$_C$	L-ADM$_{CF}$	L-ADM$_{ABC}$	q-HATM	L-ADM$_C$	L-ADM$_{CF}$	L-ADM$_{ABC}$	q-HATM	L-ADM$_C$	q-HATM
	0.2	4.13×10^{-10}	8.53×10^{-10}	1.36×10^{-9}	4.04×10^{-7}	2.74×10^{-11}	1.33×10^{-10}	2.08×10^{-10}	3.35×10^{-8}	3.32×10^{-11}	3.75×10^{-9}
	0.4	3.93×10^{-10}	6.24×10^{-10}	1.29×10^{-9}	9.87×10^{-7}	2.62×10^{-11}	1.64×10^{-10}	2.53×10^{-11}	4.02×10^{-7}	3.94×10^{-10}	8.16×10^{-8}
1	0.6	1.07×10^{-9}	1.04×10^{-9}	3.21×10^{-9}	1.28×10^{-6}	1.92×10^{-9}	1.85×10^{-9}	1.65×10^{-9}	3.36×10^{-8}	2.12×10^{-9}	5.93×10^{-7}
	0.8	7.44×10^{-9}	7.59×10^{-8}	6.88×10^{-9}	1.13×10^{-7}	8.38×10^{-9}	8.36×10^{-9}	8.11×10^{-9}	2.43×10^{-6}	8.64×10^{-9}	2.87×10^{-6}
	1.0	3.01×10^{-8}	3.04×10^{-8}	2.98×10^{-8}	7.83×10^{-6}	3.11×10^{-8}	3.11×10^{-8}	3.08×10^{-8}	1.08×10^{-5}	3.14×10^{-8}	1.14×10^{-5}
	0.2	1.39×10^{-13}	2.87×10^{-13}	4.58×10^{-13}	1.36×10^{-10}	9.77×10^{-15}	4.53×10^{-14}	7.11×10^{-14}	1.26×10^{-11}	1.02×10^{-14}	2.74×10^{-11}
	0.4	1.34×10^{-13}	2.12×10^{-13}	4.35×10^{-13}	3.31×10^{-10}	8.53×10^{-14}	5.24×10^{-14}	6.22×10^{-15}	1.35×10^{-11}	1.30×10^{-13}	1.99×10^{-10}
5	0.6	3.61×10^{-13}	3.50×10^{-13}	1.07×10^{-12}	4.31×10^{-10}	6.43×10^{-13}	6.19×10^{-13}	5.54×10^{-13}	1.29×10^{-10}	7.10×10^{-13}	9.63×10^{-10}
	0.8	2.49×10^{-12}	2.54×10^{-12}	2.30×10^{-12}	3.84×10^{-11}	2.81×10^{-12}	2.80×10^{-12}	2.72×10^{-12}	3.63×10^{-9}	2.90×10^{-12}	3.85×10^{-9}
	1.0	1.01×10^{-11}	1.02×10^{-11}	1.00×10^{-11}	2.63×10^{-9}	1.04×10^{-11}	1.04×10^{-11}	1.03×10^{-11}	3.35×10^{-8}	1.05×10^{-11}	3.75×10^{-9}

Fig. 5, Fig. 6, Fig. 7 and Table 6 and Table 7 display the numerical and graphical outcomes of **Application 2** for different fractional orders α. Fig. 5 presents the 2D plots of the exact and approximate solutions obtained by the three L-ADM formulations. The curves reveal that the approximate solutions match closely with the exact one for all values of α.

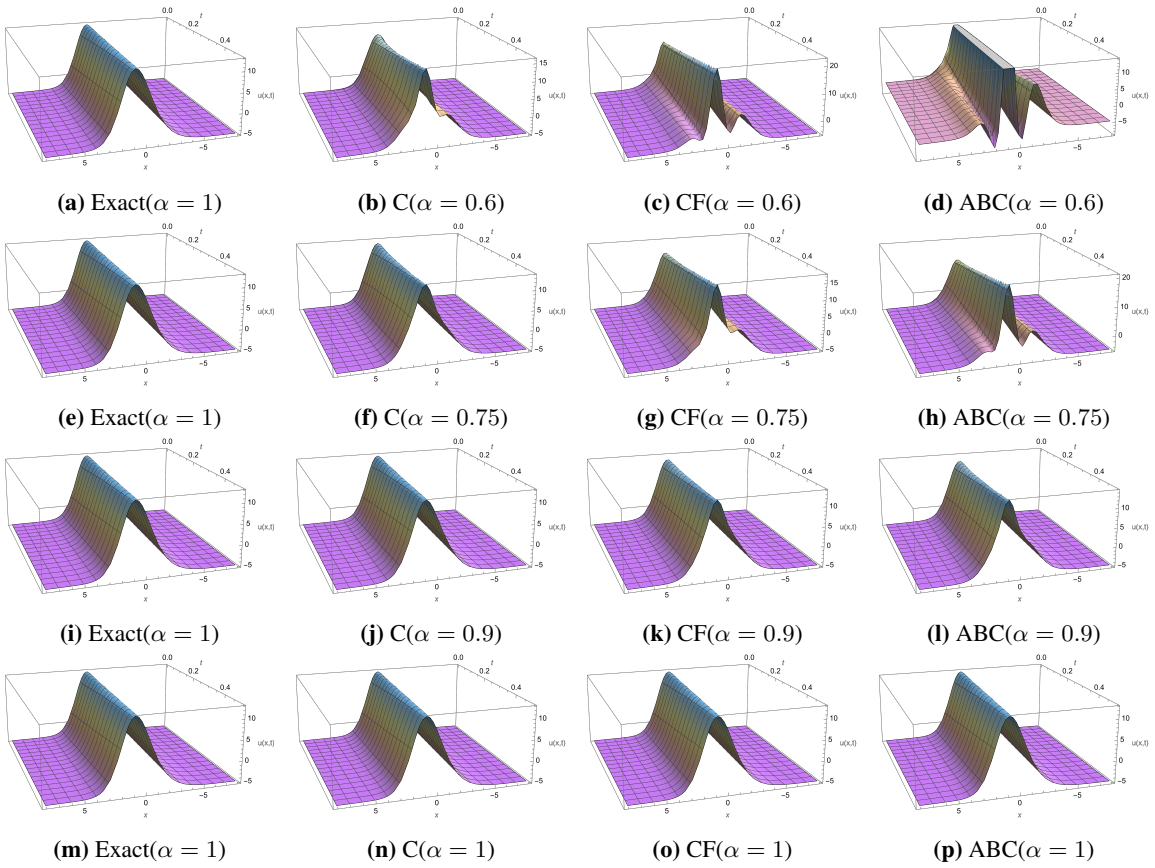

(a) Exact($\alpha = 1$) **(b)** C($\alpha = 0.6$) **(c)** CF($\alpha = 0.6$) **(d)** ABC($\alpha = 0.6$)

(e) Exact($\alpha = 1$) **(f)** C($\alpha = 0.75$) **(g)** CF($\alpha = 0.75$) **(h)** ABC($\alpha = 0.75$)

(i) Exact($\alpha = 1$) **(j)** C($\alpha = 0.9$) **(k)** CF($\alpha = 0.9$) **(l)** ABC($\alpha = 0.9$)

(m) Exact($\alpha = 1$) **(n)** C($\alpha = 1$) **(o)** CF($\alpha = 1$) **(p)** ABC($\alpha = 1$)

Fig. 6. 3D plots of the exact and third-order approximate solutions obtained by L-ADM$_C$, L-ADM$_{CF}$, and L-ADM$_{ABC}$ in Application 2 at Different values of α, with $-8 \leq \zeta \leq 8$, and $0 \leq \varrho \leq 0.5$, where $a_1 = 1$, $a_2 = \frac{1}{2}$, and $a_3 = 1$

As α decreases, the wave amplitude becomes smaller and the oscillations are more damped, illustrating the strong memory and diffusion effects introduced by the fractional derivatives. The Caputo formulation exhibits the most accurate and smooth profile, while Caputo-Fabrizio shows slightly slower variations, and Atangana–Baleanu (Caputo sense) gives the flattest and most diffusive wave behavior.

This trend highlights that the singular kernel of Caputo retains sharper local dynamics, whereas the non-singular kernels of Caputo-Fabrizio and Atangana-Baleanu (Caputo sense) spread the influence of past states more evenly, resulting in smoother wave shapes. Overall, the decrease in α controls the rate of damping and diffusion in the wave propagation process.

Fig. 6 shows the 3D surfaces of the exact and approximate solutions of L-ADM. The surfaces obtained by all three L-ADM variants are in very close agreement with the exact analytical solution, confirming the robustness and reliability of the proposed approach. When α is reduced, the surface peaks become flatter and smoother, demonstrating the enhanced diffusion and energy dissipation caused by the fractional-order effect. The Caputo derivative again provides the most stable and physically consistent surface, while the Caputo-Fabrizio and Atangana-Baleanu (Caputo sense) forms display broader and more diffusive wave fronts due to their weaker short-term memory effects.

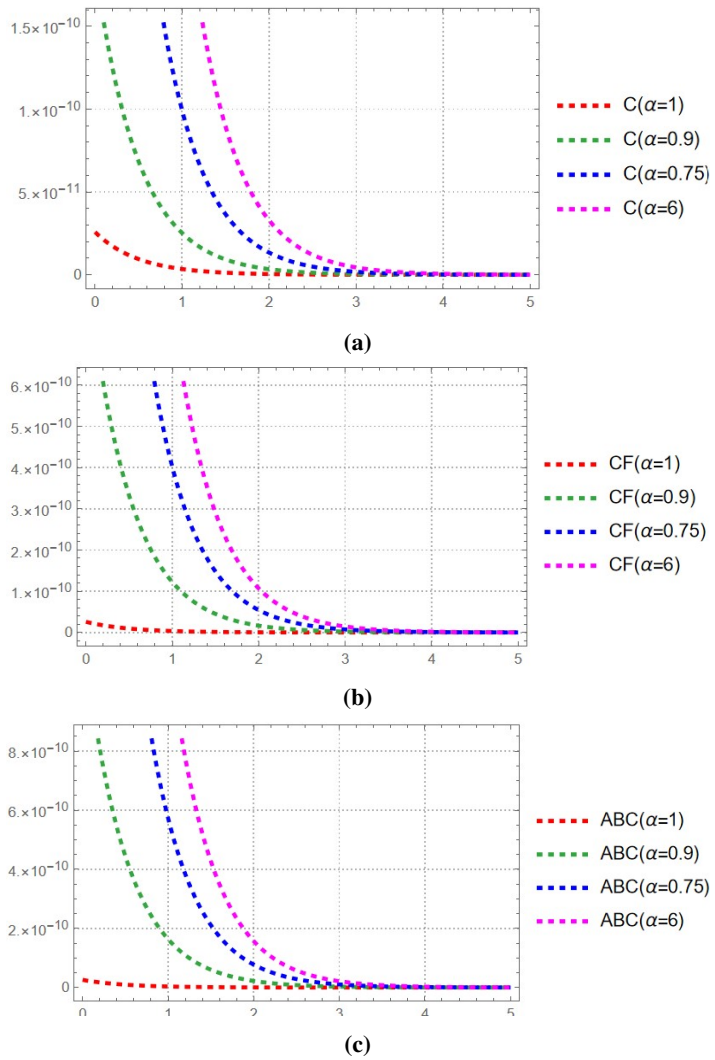

Fig. 7. 2D graphs of the absolute errors of the third-order approximations for L-ADM$_C$, L-ADM$_{CF}$, and L-ADM$_{ABC}$ in Application 2, at different values of α, for $0 \leq \zeta \leq 5$, and with $\varrho = 0.1$, where $a_1 = 3$, $a_2 = \frac{1}{2}$, and $a_3 = -13$

This observation confirms that the variation of α significantly influences the balance between nonlinearity and dispersion in the fractional KS system, with higher α values producing sharper waves and lower α values yielding smoother transitions. Fig. 7 depicts the 2D distributions of the absolute errors for the three fractional derivatives. The results demonstrate that the numerical errors remain small across the spatial domain, verifying the accuracy and convergence of the method.

The Caputo version consistently produces the smallest errors, followed by Caputo-Fabrizio and then Atangana-Baleanu (Caputo sense), which again corresponds to the precision hierarchy observed in Application 1. As α decreases, a slight increase in error is observed because the fractional memory becomes stronger, but the overall deviation remains negligible. This confirms that the L-ADM provides highly stable and accurate approximations for the fractional KS problem under all derivative definitions.

Table 6 gives a detailed numerical comparison of the approximations obtained by L-ADM for the three fractional derivatives and by the q-HATM method [61]. It can be seen that the errors produced by L-ADM are smaller than those obtained by q-HATM for all α values. The Caputo version once again achieves the highest precision, followed by Caputo-Fabrizio and Atangana-Baleanu (Caputo sense),

which maintain smooth but slightly less accurate solutions. This clearly demonstrates the advantage of the L-ADM in producing reliable and precise results with fewer computational steps.

Table 7 further supports these findings by reporting the absolute error values for various fractional orders. All three L-ADM formulations yield errors on the order of 10^{-7} or less, confirming rapid convergence and high numerical efficiency. Although minor differences appear as α decreases, the L-ADM remains superior in both accuracy and simplicity compared with q-HATM. The Caputo derivative provides the most accurate results, while the non-singular kernel derivatives offer smoother behavior with minimal deviation. These findings highlight the flexibility and robustness of the proposed L-ADM approach for solving nonlinear fractional equations involving different derivative definitions.

6. Summary and Conclusions

In this study, the L-ADM was effectively applied to the nonlinear time-fractional KS equation using three different definitions of the fractional derivative: Caputo, Caputo–Fabrizio, and Atangana–Baleanu (Caputo sense). The comparative analysis of these operators revealed important insights into how the memory kernels influence the dynamics of fractional systems. The results demonstrated that the Caputo formulation yields the highest accuracy and smoothest convergence behavior, preserving the main wave features of the KS system. The Caputo–Fabrizio derivative, characterized by its exponential kernel, provides slightly smoother and more diffusive profiles, while the Atangana–Baleanu (Caputo sense) derivative exhibits the strongest damping effect due to its Mittag–Leffler kernel. This ranking highlights that the choice of kernel significantly affects the balance between local precision and global diffusion in fractional models.

Across all test cases, the L-ADM showed excellent numerical stability, fast convergence, and strong agreement between analytical and approximate solutions. The method proved more accurate and computationally efficient than other recent techniques such as NTDM and q-HATM, confirming its robustness for nonlinear fractional problems.

However, some limitations should be noted. The computational cost increases with higher-order approximations, especially for strongly nonlinear or multi-dimensional problems. In addition, the convergence rate may slow down when the fractional order α becomes very small due to the dominance of long-memory effects. These aspects suggest that adaptive schemes or hybrid numerical–analytical approaches could further enhance performance in future implementations.

Overall, this work not only validates the capability of L-ADM to handle nonlinear FPDEs but also clarifies the physical and numerical distinctions among different fractional derivatives. Future research may extend this study to multi-dimensional systems, fractional-order control models, dynamical simulations, and robotics applications, as well as to problems involving complex boundary conditions or real-world data.

Author Contribution: All authors contributed equally to the main contributor to this paper. All authors read and approved the final paper.

Funding: This research received no external funding.

Conflicts of Interest: The authors declare no conflict of interest.

References

[1] G. A. Anastassiou, *Generalized Fractional Calculus*, Spring Cham, 2021, https://doi.org/10.1007/978-3-030-56962-4.

[2] J. E. Macías-Díaz, "Fractional Calculus—theory and Applications," *Axioms*, vol. 11, no. 2, p. 43, 2022, https://doi.org/10.3390/axioms11020043.

[3] R. Agarwal, S. D. Purohit, and Kritika, "Introduction to fractional calculus and modelling," *in Modeling*

Calcium Signaling, pp. 1–28, 2024, https://doi.org/10.1007/978-981-97-1651-7_1.

[4] O. Jawabreh *et al*., "Fractional calculus analysis of tourism mathematical model," *Progress in Fractional Differentiation and Applications*, vol. 9, pp. 1–11, 2023, https://doi.org/10.18576/pfda/09S101.

[5] M. Kostić, "Multidimensional fractional calculus: Theory and applications," *Axioms*, vol. 13, no. 9, p. 623, 2024, https://doi.org/10.3390/axioms13090623.

[6] A. S. Hussain, K. D. Pati, A. K. Atiyah, and M. A. Tashtoush, "Rate of occurrence estimation in geometric processes with Maxwell distribution: a comparative study between artificial intelligence and classical methods," *International Journal of Advances in Soft Computing and its Application*, vol. 17, no. 1, pp. 1–15, 2025, https://doi.org/10.15849/IJASCA.250330.01.

[7] P. Singh, N. Zade, P. Priyadarshi, and A. Gupte, "The application of machine learning and deep learning techniques for global energy utilization projection for ecologically responsible energy management," *International Journal of Advances in Soft Computing and its Application*, vol. 16, no. 3, pp. 49–66, 2025, https://doi.org/10.15849/IJASCA.250330.04.

[8] M. Berir, "Analysis of the effect of white noise on the Halvorsen system of variable-order fractional derivatives using a novel numerical method," *International Journal of Advances in Soft Computing and its Application*, vol. 16, no. 3, pp. 294–306, 2024, https://doi.org/10.15849/IJASCA.241130.16.

[9] T. Hamadneh, A. Hioual, O. Alsayyed, Y. A. Al-Khassawneh, A. Al-Husban, and A. Ouannas, "Finite time stability results for neural networks described by variable-order fractional difference equations," *Fractal and Fractional*, vol. 7, no. 8, p. 616, 2023, https://doi.org/10.3390/fractalfract7080616.

[10] A. Jameel, N. R. Anakira, A. K. Alomari, I. Hashim, and M. A. Shakhatreh, "Numerical solution of nth-order fuzzy initial value problems by six stages," *Journal of Nonlinear Science and Applications*, vol. 9, no. 2, pp. 627–640, 2016, https://doi.org/10.22436/jnsa.009.02.26.

[11] A. F. Jameel, N. Anakira, A. K. Alomari, I. Hashim, and S. Momani, "A new approximation method for solving fuzzy heat equations," *Journal of Computational and Theoretical Nanoscience*, vol. 13, pp. 7825–7832, 2016, https://www.researchgate.net/profile/Ali-Jameel-2/publication/312488842_A_New_Approximation_Method_for_Solving_Fuzzy_Heat_Equations/links/5b0266f04585154aeb061731/A-New-Approximation-Method-for-Solving-Fuzzy-Heat-Equations.pdf.

[12] M. D'Elia and C. Glusa, "A fractional model for anomalous diffusion with increased variability: Analysis, algorithms and applications to interface problems," *Numerical Methods for Partial Differential Equations*, vol. 38, no. 6, pp. 2084–2103, 2022, https://doi.org/10.1002/num.22865.

[13] L. R. Evangelista and E. K. Lenzi, "Fractional anomalous diffusion," in *An Introduction to Anomalous Diffusion and Relaxation, Cham: Springer*, pp. 189–236, 2023, https://doi.org/10.1007/978-3-031-18150-4_5.

[14] C. Lim and J. H. Jeon, "Anomalous diffusion in coupled viscoelastic media: A fractional Langevin equation approach," *arXiv preprint*, 2025, https://doi.org/10.48550/arXiv.2507.08291.

[15] M. L. -Varas *et al*., "Viscoelasticity modelling of asphalt mastics under permanent deformation through the use of fractional calculus," *Construction and Building Materials*, vol. 329, p. 127102, 2022, https://doi.org/10.1016/j.conbuildmat.2022.127102.

[16] A. O. Alshammari, "Dynamical behavior of a time-fractional biological model via an efficient numerical method," *Journal of Applied Mathematics and Computing*, vol. 71, no. 2, pp. 2543–2569, 2025, https://doi.org/10.1007/s12190-024-02329-4.

[17] W. Chen, H. Sun, and X. Li, *Fractional Derivative Modeling in Mechanics and Engineering*, Springer Nature, 2022, https://doi.org/10.1007/978-981-16-8802-7.

[18] M. A. Hussein, "The Approximate Solutions of Fractional Differential Equations with Antagana-Baleanu Fractional Operator," *Mathematics and Computional Sciences*, vol. 3, no. 3, pp. 29–39, 2022, https://doi.org/10.30511/mcs.2022.560414.1077.

[19] H. M. Srivastava, W. Adel, M. Izadi, and A. A. El-Sayed, "Solving some physics problems involving fractional-order differential equations with the Morgan–Voyce polynomials," *Fractal and Fractional*, vol. 7, no. 4, p. 301, 2023, https://doi.org/10.3390/fractalfract7040301.

[20] I. Siddique, A. M. Mirza, K. Shahzadi, M. A. Akbar, and F. Jarad, "Diverse precise traveling wave solutions possessing beta derivative of the fractional differential equations arising in mathematical physics," *Journal of Function Spaces*, vol. 2022, 2022, https://doi.org/10.1155/2022/5613708.

[21] M. A. Khan and A. Atangana, *Numerical Methods for Fractal-Fractional Differential Equations and Engineering: Simulations and Modeling*, CRC Press, 2023, https://doi.org/10.1201/9781003359258.

[22] T. Abdeljawad *et al*., "Analysis of a class of fractal hybrid fractional differential equation with application to a biological model," *Scientific Reports*, vol. 14, no. 18937, 2024, https://doi.org/10.1038/s41598-024-67158-8.

[23] K. Hattaf, "On the stability and numerical scheme of fractional differential equations with application to biology," *Computation*, vol. 10, no. 6, p. 97, 2022, https://doi.org/10.3390/computation10060097.

[24] D. M. Michelson, G. I. Sivashinsky, "Nonlinear analysis of hydrodynamic instability in laminar flames—II. Numerical experiments," *Acta Astronautica*, vol. 4, no. 11–12, pp. 1177–1206, 1977, https://doi.org/10.1016/0094-5765(77)90097-2.

[25] Y. Kuramoto, "Diffusion-induced chaos in reaction systems," *Progress of Theoretical Physics Supplement*, vol. 64, pp. 346–367, 1978, https://doi.org/10.1143/PTPS.64.346.

[26] R. J. Tomlin, S. N. Gomes, G. A. Pavliotis, and D. T. Papageorgiou, "Optimal control of thin liquid films and transverse mode effects," *SIAM Journal on Applied Dynamical Systems*, vol. 18, no. 1, pp. 117–149, 2019, https://doi.org/10.1137/18M1193906.

[27] C. M. Linares *et al*., "A machine learning approach to bridge the gap between the Kuramoto–Sivashinsky and the Navier–Stokes equations for thin film flow," in *Aiche Annual Meeting*, 2022, https://aiche.confex.com/aiche/2022/meetingapp.cgi/Paper/649364.

[28] G. M. Coclite and L. di Ruvo, "On the Solutions for the Conserved Kuramoto–Sivashinsky Equation," *Milan Journal of Mathematics*, vol. 93, pp. 75–107, 2025, https://doi.org/10.1007/s00032-025-00413-3.

[29] M. Enlow, A. Larios, and J. Wu, "Algebraic calming for the 2D Kuramoto–Sivashinsky equations," *Nonlinearity*, vol. 37, no. 11, p. 115019, 2024, https://doi.org/10.1088/1361-6544/ad792e.

[30] N. A. Kudryashov and S. F. Lavrova, "Dynamical features of the generalized Kuramoto–Sivashinsky equation," *Chaos, Solitons & Fractals*, vol. 142, p. 110502, 2021, https://doi.org/10.1016/j.chaos.2020.110502.

[31] E. Özalp, G. Margazoglou, and L. Magri, "Reconstruction, forecasting, and stability of chaotic dynamics from partial data," *Chaos: An Interdisciplinary Journal of Nonlinear Science*, vol. 33, 2023, https://doi.org/10.1063/5.0159479.

[32] M. Abadie, P. Beck, J. P. Parker, and T. M. Schneider, "The topology of a chaotic attractor in the Kuramoto–Sivashinsky equation," *Chaos: An Interdisciplinary Journal of Nonlinear Science*, vol. 35, 2025, https://doi.org/10.1063/5.0237476.

[33] E. Özalp and L. Magri, "Stability analysis of chaotic systems in latent spaces," *Nonlinear Dynamics*, vol. 113, no. 11, pp. 13791–13806, 2025, https://doi.org/10.1007/s11071-024-10712-w.

[34] M. S. Alam, W. Ott, and I. Timofeyev, "Attractor learning for spatiotemporally chaotic dynamical systems using echo state networks with transfer learning," *arXiv preprint*, 2025, https://doi.org/10.48550/arXiv.2505.24099.

[35] O. Ersoy Hepson, "Numerical simulations of Kuramoto–Sivashinsky equation in reaction–diffusion via Galerkin method," *Mathematical Sciences*, vol. 15, no. 2, 2021, https://doi.org/10.1007/s40096-021-00402-8.

[36] S. R. Jena and G. S. Gebremedhin, "Numerical treatment of Kuramoto–Sivashinsky equation on B-spline collocation," *Arab Journal of Basic and Applied Sciences*, vol. 28, no. 1, pp. 283–291, 2021, https://doi.org/10.1080/25765299.2021.1949846.

[37] N. Kaur and V. Joshi, "Kuramoto–Sivashinsky equation: Numerical solution using two quintic B-splines and differential quadrature method," *Mathematics and Computers in Simulation*, vol. 220, pp. 105–127, 2024, https://doi.org/10.1016/j.matcom.2023.12.036.

[38] S. Albosaily, W. W. Mohammed, A. Rezaiguia, M. El-Morshedy, and E. M. Elsayed, "The influence of the noise on the exact solutions of a Kuramoto–Sivashinsky equation," *Open Mathematics*, vol. 20, no. 1, pp. 108–116, 2022, https://doi.org/10.1515/math-2022-0012.

[39] P. Veeresha and D. G. Prakasha, "Solution for fractional Kuramoto–Sivashinsky equation using novel computational technique," *International Journal of Applied and Computational Mathematics*, vol. 7, no. 33, 2021, https://doi.org/10.1007/s40819-021-00956-0.

[40] M. Nadeem and L. F. Iambor, "Advanced Numerical Scheme for Solving Nonlinear Fractional Kuramoto–Sivashinsky Equations Using Caputo Operators," *Fractal and Fractional*, vol. 9, no. 7, p. 418, 2025, https://doi.org/10.3390/fractalfract9070418.

[41] Ö. Avit and H. Anac, "The novel numerical solutions for conformable fractional Kuramoto–Sivashinsky equations by using Cq-HATM and CHPETM," *Alexandria Engineering Journal*, vol. 92, pp. 294–309, 2024, https://doi.org/10.1016/j.aej.2024.01.027.

[42] H. P. Bhatt and A. Chowdhury, "A high-order implicit–explicit Runge–Kutta type scheme for the numerical solution of the Kuramoto–Sivashinsky equation," *International Journal of Computer Mathematics*, vol. 98, no. 6, pp. 1254–1273, 2021, https://doi.org/10.1080/00207160.2020.1814262.

[43] M. Hosseininia *et al*., "A numerical method based on the Chebyshev cardinal functions for variable-order fractional version of the fourth-order 2D Kuramoto–Sivashinsky equation," *Mathematical Methods in the Applied Sciences*, vol. 44, no. 2, pp. 1831–1842, 2021, https://doi.org/10.1002/mma.6881.

[44] M. K. Iqbal, M. Abbas, T. Nazir, and N. Ali, "Application of new quintic polynomial B-spline approximation for numerical investigation of Kuramoto–Sivashinsky equation," *Advances in Difference Equations*, vol. 2020, no. 558, 2020, https://doi.org/10.1186/s13662-020-03007-y.

[45] A. Shah and S. Hussain, "An analytical approach to the new solution of family of Kuramoto–Sivashinsky equation by q-Homotopy Analysis Technique," *International Journal of Differential Equations*, vol. 2024, pp. 1–11, 2024, https://doi.org/10.1155/2024/6652990.

[46] M. M. Al-Sawalha *et al*., "Analytical solutions to time–space fractional Kuramoto–Sivashinsky model using the integrated Bäcklund transformation and Riccati–Bernoulli sub-ODE method," *AIMS Mathematics*, vol. 9, no. 5, pp. 12357–12374, 2024, https://doi.org/10.3934/math.2024604.

[47] R. K. Mohanty and D. Sharma, "A new 2-level implicit high accuracy compact exponential approximation for the numerical solution of nonlinear fourth order Kuramoto–Sivashinsky and Fisher–Kolmogorov equations," *Journal of Mathematical Chemistry*, vol. 62, no. 5, pp. 973–1011, 2024, https://doi.org/10.1007/s10910-024-01577-w.

[48] N. H. Tuan, H. Mohammadi, and S. Rezapour, "A mathematical model for COVID-19 transmission by using the Caputo fractional derivative," *Chaos, Solitons & Fractals*, vol. 140, p. 110107, 2020, https://doi.org/10.1016/j.chaos.2020.110107.

[49] O. Brandibur, R. Garrappa, and E. Kaslik, "Stability of systems of fractional-order differential equations with Caputo derivatives," *Mathematics*, vol. 9, no. 8, p. 914, 2021, https://doi.org/10.3390/math9080914.

[50] Y. Mahatekar, P. S. Scindia, and P. Kumar, "A new numerical method to solve fractional differential equations in terms of Caputo–Fabrizio derivatives," *Physica Scripta*, vol. 98, no. 024001, 2023, https://doi.org/10.1088/1402-4896/acaf1a.

[51] N. Almutairi and S. Saber, "On chaos control of nonlinear fractional Newton–Leipnik system via fractional Caputo–Fabrizio derivatives," *Scientific Reports*, vol. 13, no. 22726, 2023, https://doi.org/10.1038/s41598-023-49541-z.

[52] C. Liu, C. Yu, Z. Gong, H. T. Cheong, and K. L. Teo, "Numerical computation of optimal control problems with Atangana–Baleanu fractional derivatives," *Journal of Optimization Theory and Applications*, vol. 197, no. 2, pp. 798–816, 2023, https://doi.org/10.1007/s10957-023-02212-5.

[53] A. Omame and F. D. Zaman, "Solution of the modified time fractional coupled Burgers equations using Laplace Adomian decomposition method," *Acta Mechanica et Automatica*, vol. 17, no. 1, pp. 124–132, 2023, https://doi.org/10.2478/ama-2023-0014.

[54] N. A. Sheikh, F. Ali, M. Saqib, I. Khan, and S. A. A. Jan, "A comparative study of Atangana–Baleanu and Caputo–Fabrizio fractional derivatives to the convective flow of a generalized Casson fluid," *The European Physical Journal Plus*, vol. 132, no. 54, 2017, https://doi.org/10.1140/epjp/i2017-11326-y.

[55] A. Khan, K. A. Abro, A. Tassaddiq, and I. Khan, "Atangana–Baleanu and Caputo–Fabrizio analysis of fractional derivatives for heat and mass transfer of second grade fluids over a vertical plate: A comparative study," *Entropy*, vol. 19, no. 8, p. 279, 2017, https://doi.org/10.3390/e19080279.

[56] N. A. Sheikh *et al*., "Comparison and analysis of the Atangana–Baleanu and Caputo–Fabrizio fractional derivatives for generalized Casson fluid model with heat generation and chemical reaction," *Results in Physics*, vol. 7, pp. 789–800, 2017, https://doi.org/10.1016/j.rinp.2017.01.025.

[57] S. Noor, W. Albalawi, M. Alqudah, R. Shah, and S. A. El-Tantawy, "Efficient Solutions for Fractional Order Kuramoto–Sivashinsky Equation: Aboodh Residual Power Series Method," *Contemporary Mathematics*, pp. 6586–6609, 2025, https://doi.org/10.37256/cm.6520255269.

[58] A. Kumar, "Dynamic behaviour and semi-analytical solution of nonlinear fractional-order Kuramoto–Sivashinsky equation," *Pramana*, vol. 98, no. 2, p. 48, 2024, https://doi.org/10.1007/s12043-024-02728-z.

[59] M. M. Al-Sawalha *et al.*, "Analytical solutions to time–space fractional Kuramoto–Sivashinsky model using the integrated Bäcklund transformation and Riccati–Bernoulli sub-ODE method," *AIMS Mathematics*, vol. 9, no. 5, pp. 12357–12374, 2024, https://doi.org/10.3934/math.2024604.

[60] A. S. Alshehry, M. Imran, A. Khan, and W. Weera, "Fractional view analysis of Kuramoto–Sivashinsky equations with non-singular kernel operators," *Symmetry*, vol. 14, no. 7, p. 1463, 2022, https://doi.org/10.3390/sym14071463.

[61] P. Veeresha and D. G. Prakasha, "Solution for fractional Kuramoto–Sivashinsky equation using novel computational technique," *International Journal of Applied and Computational Mathematics*, vol. 7, no. 2, p. 33, 2021, https://doi.org/10.1007/s40819-021-00956-0.

[62] M. S. Sebaq, A. H. Qamlo, and G. M. Bahaa, "Numerical solutions for fractional optimal control problems of coupled diffusion systems via Laplace Adomian Decomposition Method," *Boundary Value Problems*, vol. 2025, no. 131, 2025, https://doi.org/10.1186/s13661-025-02108-5.

[63] A. O. Yunus, M. O. Olayiwola, M. A. Omoloye, and A. O. Oladapo, "A fractional-order model of Lassa disease using the Laplace-Adomian decomposition method," *Healthcare Analytics*, vol. 3, p. 100167, 2023, https://doi.org/10.1016/j.health.2023.100167.

[64] O. Nave, U. Shemesh, and I. HarTuv, "Applying Laplace Adomian decomposition method (LADM) for solving a model of COVID-19," *Computer Methods in Biomechanics and Biomedical Engineering*, vol. 24, no. 14, pp. 1618–1628, 2021, https://doi.org/10.1080/10255842.2021.1904399.

[65] N. Jeeva and K. M. Dharmalingam, "Mathematical analysis of new SEIQR model via Laplace Adomian decomposition method," *Indian Journal of Natural Sciences*, vol. 15, no. 83, pp. 72148–72157, 2024, https://www.researchgate.net/profile/N-Jeeva/publication/381853011_Mathematical_Analysis_of_New_SEIQR_Model_via_Laplace_Adomian_Decomposition_Method/links/668260972aa57f3b8264353b/Mathematical-Analysis-of-New-SEIQR-Model-via-Laplace-Adomian-Decomposition-Method.pdf.

[66] A. Omame and F. D. Zaman, "Solution of the modified time-fractional coupled Burgers equations using Laplace Adomian decomposition method," *Acta Mechanica et Automatica*, vol. 17, no. 1, pp. 124–132, 2023, https://doi.org/10.2478/ama-2023-0014.